

Infrared Dark Cloud Cores in the SCUBA Legacy Catalogue

H. Parsons^{1*}, M. A. Thompson^{1†} and A. Chrysostomou^{1,2}

¹Centre for Astrophysics Research, Science & Technology Research Institute,
University of Hertfordshire, College Lane, Hatfield, AL10 9AB, UK

²Joint Astronomy Centre, 660 North A’ohoku Place, University Park, Hilo, Hawaii 96720, U.S.A.

Accepted 2009 July 7. Received 2009 July 7; in original form 2009 March 13

ABSTRACT

We present an investigation of candidate Infrared Dark Cloud cores as identified by Simon et al. (2006) located within the SCUBA Legacy Catalogue. After applying a uniform noise cut to the Catalogue data we identify 154 Infrared Dark Cloud cores that were detected at 850 μm and 51 cores that were not. We derive column densities for each core from their 8 μm extinction and find that the IRDCs detected at 850 μm have higher column densities (a mean of $1.7 \times 10^{22} \text{ cm}^{-2}$) compared to those cores not detected at 850 μm (a mean of $1.0 \times 10^{22} \text{ cm}^{-2}$). Combined with sensitivity estimates, we suggest that the cores not detected at 850 μm are low mass, low column density and low temperature cores that are below the sensitivity limit of SCUBA at 850 μm . For a subsample of the cores detected at 850 μm those contained within the MIPS GAL area) we find that two thirds are associated with 24 μm sources. Cores not associated with 24 μm emission are either “starless” IRDC cores that perhaps have yet to form stars, or contain low mass YSOs below the MIPS GAL detection limit. We see that those “starless” IRDC cores and the IRDC cores associated with 24 μm emission are drawn from the same column density population and are of similar mass. If we then assume the cores without 24 μm embedded sources are at an earlier evolutionary stage to cores with embedded objects we derive a statistical lifetime for the quiescent phase of a few 10^3 – 10^4 years. Finally, we make conservative predictions for the number of observed IRDCs that will be observed by the Apex Telescope Galactic Plane Survey (ATLAS GAL), the Herschel Infrared Galactic Plane Survey (Hi-GAL), the JCMT Galactic Plane Survey (JPS) and the SCUBA-2 “All Sky” Survey (SASSy).

Key words: stars: formation – dust –infrared: ISM – submillimetre

1 INTRODUCTION

Infrared Dark Clouds (IRDCs) were first observed in the mid-1990s by the Infrared Space Observatory, ISO, (Perault et al. 1996) and the Midcourse Space eXperiment, MSX, (Egan et al. 1998) as silhouettes against the bright mid-infrared Galactic background. Initially, Egan et al. (1998) identified ~ 2000 clouds by eye from the MSX Galactic Plane Survey images. A systematic study of the MSX data using an automated identification process by Simon et al. (2006) identified 10,931 candidate IRDCs within which a total of 12,774 compact IRDC core candidates were detected. By definition each IRDC contains at least one core.

An unsurprising consequence of this detection method

is the fact that the Galactic distribution of IRDCs follows the mid-infrared background of the Galaxy. IRDCs are predominantly found in the first and fourth Galactic quadrants and near to the Galactic mid-plane (Jackson et al. 2008), precisely where the mid-infrared background is greatest. Simon et al. (2006) used data from the Galactic Ring Survey (GRS) to obtain distance estimates for IRDCs found within the first quadrant of the Galaxy, using a morphological match with ^{13}CO emission. This matching process identified distances to 313 candidate IRDCs. Further distance estimates have been obtained by Jackson et al. (2008) for 316 IRDC candidates contained within the fourth quadrant and were obtained using single pointings of CS ($J=2-1$). The distances obtained from these large scale investigations show a peak in the radial galactocentric distribution of IRDCs corresponding to the location of the Scutum-Centaurus arm i.e. peak of $R=5\text{kpc}$ in the first quadrant and $R=6\text{kpc}$ in the fourth (Jackson et al. 2008).

* E-mail: H.A.L.Parsons@Herts.ac.uk;

† E-mail: M.A.Thompson@Herts.ac.uk;

In the decade since their discovery, our understanding of the physical properties of IRDCs has increased and it is now known that these objects are cold ($<25\text{ K}$) dense (10^5 cm^{-3}) regions, on scales of 1–10 pc, with masses ranging between 10^2 – $10^5 M_\odot$ (Rathborne et al. 2006). Current theory suggests that cold dense starless cores found within IRDCs are the precursors to hot molecular cores (Jackson et al. 2008 and references therein), indeed Rathborne et al. (2007) report on a hot molecular core found within an IRDC. Other tracers of massive star formation such as HII regions and Class II methanol (CH_3OH) masers (Carey et al. 1998; Pillai et al. 2006; Chambers et al. (2009)) have been found in association with a number of IRDCs. The association with high mass star formation is not exclusive: a number of individual studies find only low to intermediate mass young stellar objects embedded within IRDCs (van der Wiel & Shipman 2008).

To date, with the exception of distance estimates, only small samples of the IRDCs originally published by Simon et al. (2006) have been investigated, with an observational bias towards the darkest high contrast clouds (Rathborne et al. 2006; Du & Yang 2008). The trends of global properties across a large sample of IRDCs have yet to be investigated, in particular the proportion of IRDCs that are associated with active star formation as opposed to IRDCs that are quiescent or starless.

This paper aims to address this issue by studying candidate IRDC cores originally identified by Simon et al. (2006) that are contained within the recently published SCUBA Legacy Catalogue by Di Francesco et al. (2008). In Section 2 we describe the cross matching method used on the two catalogues, obtain column density and mass estimates (or upper limits where applicable) and identify $24\text{ }\mu\text{m}$ embedded sources associated with the the cores identified. The results of the cross matching procedure are presented in Section 3. We discuss our findings in Section 4 with a mention of the impact on two of the forthcoming James Clerk Maxwell Telescope¹ (JCMT) Legacy surveys. Finally we make some concluding remarks in Section 5.

2 CROSS-MATCHING IRDCS IN MSX, SCUBA AND MIPS GAL

2.1 Archival data

In 2006, Simon et al. produced a catalogue of 10,931 candidate IRDCs using data from the MSX satellite that covered the entire Galactic plane from $l=0-360^\circ$ and $|b|\leq 5^\circ$. Candidate IRDCs were identified by modelling the Galactic background diffuse emission at $8\text{ }\mu\text{m}$, subtracting the $8\text{ }\mu\text{m}$ MSX images from this model and then dividing by the background model to produce what is known as a “contrast image”. Regions of high extinction in the raw images appeared as positive objects with contrast values between 0 and 1 (1 for highly extincted objects) in the contrast images. IRDCs were then identified by looking for extended contrast

sources, those with 36 or more continuous pixels with a contrast greater than 2σ . Cores within the clouds were identified by decomposing the clouds using two-dimensional elliptical Gaussian fits (Simon et al. 2006). Although discovered by their mid-infrared absorption, it is at sub millimetre and far-infrared wavelengths that these objects have their peak emission.

Di Francesco et al. (2008) present a comprehensive re-reduction of the entire 8 year sub millimetre continuum data set observed by SCUBA (Sub millimetre Common User Bolometer Array) on the JCMT in Hawaii. This data set is known as the SCUBA Legacy Catalogue and covers a total area of just over 29 square degrees at $850\text{ }\mu\text{m}$. A consequence of the varying weather conditions and method by which the data was collected, over the entire lifetime of SCUBA, is that the data within the SCUBA Legacy Catalogue is both non-uniform in noise and in its quality of opacity corrections. Di Francesco et al. (2008) divided the SCUBA Legacy Catalogue into a Fundamental and an Extended Dataset. The former uses data for which there is well known atmospheric opacity calibration data (from both skydips and the CSO radiometer, Di Francesco et al. 2008) and the latter contains all observations regardless of the data quality. Coverage by the Extended data set is greater in area than the Fundamental by 9.7 square degrees. Discrete objects were identified within the SCUBA Legacy Catalogue (from both the Fundamental and Extended Dataset independently) using Clumpfind² (Di Francesco et al. 2008). This process provides information on the properties of each object such as flux (at the peak and integrated over its area) and apparent size.

MIPSGAL³ is a survey of the Galactic Plane from $10 < l < 65^\circ$ and $-10 > b > -65^\circ$ $|b| < 1^\circ$ at 24 and $70\text{ }\mu\text{m}$, using the MIPS instrument on Spitzer⁴. As a tracer of warm dust and with good resolution ($6''$ angular resolution as opposed to $20''$ and $14''$ for MSX and SCUBA respectively), MIPSGAL $24\text{ }\mu\text{m}$ data are ideal for investigating warm embedded objects, such as Young Stellar Objects. Indeed Frieswijk et al. (2008) combined MIPSGAL data with IRAC (Infrared Camera on Spitzer), 2MASS (Two Micron All Sky Survey) and SCUBA data to identify Young Stellar Objects (YSOs) within IRDC MSXDC G048.65-00.29.

2.2 Cross identification

In total, 428 MSX IRDC cores from Simon et al. (2006) were located in regions mapped by SCUBA (325 located in the Fundamental region and an additional 103 located in the Extended region). However the SCUBA Legacy Catalogue does not contain photometric measurements of objects located at the edges of maps (which may be subject to large scale background or noise fluctuations). In addition, regions of high noise persist within the catalogue due to the

² The Clumpfind algorithm used to identify objects was adapted from Williams et al. (1994) (Di Francesco et al. 2008).

³ MIPS (Multiband Imaging Photometer for Spitzer) Galactic Plane Survey. Data available from <http://irsa.ipac.caltech.edu/data/SPITZER/MIPSGAL/images/>

⁴ The Spitzer Space Telescope is operated by the Jet Propulsion Laboratory, California Institute of Technology under NASA contract 1407.

¹ The James Clerk Maxwell Telescope is operated by the Joint Astronomy Centre on behalf of the Scientific and Technology Facilities Council of the UK, the Netherlands Association for Scientific Research, and the National Research Council of Canada.

non-uniform way in which the data were taken. In order to make the catalogue more uniform we exclude data with an rms noise greater than $0.1 \text{ Jy pixel}^{-1}$, the pixel size for data in the SCUBA Legacy Catalogue is $6''$. This $0.1 \text{ Jy pixel}^{-1}$ cut excludes the high noise Poisson tail present in the data (Di Francesco et al. 2008) and gives the remaining data approximately Gaussian noise statistics, with a mean and sigma of $0.05 \text{ Jy pixel}^{-1}$ and $0.024 \text{ Jy pixel}^{-1}$ respectively. Taking map edges into account and excluding regions with noise $> 0.1 \text{ Jy pixel}^{-1}$ leaves us with 251 MSX IRDC cores within the SCUBA Legacy Catalogue mapped region. The 251 MSX candidate IRDC cores were then cross matched to sources identified within the SCUBA Legacy Catalogue (as defined by Clumpfind). IRDC cores were matched against both the Fundamental and the Extended data Catalogues.

For the cross identification process, the locations of the MSX IRDC cores were positionally matched using TOPCAT⁵ to the locations of the Clumpfind SCUBA objects. The irregular morphology of the candidate objects in both the MSX $8 \mu\text{m}$ contrast images and the SCUBA $850 \mu\text{m}$ emission maps, meant that the task of cross matching cores between the two catalogues was non trivial. Simon et al. (2006) identified IRDCs within the MSX $8 \mu\text{m}$ data as contiguous structures in the contrast images that were sufficiently extended to be real clouds and not artifacts. The cores within the clouds were identified using two dimensional elliptical Gaussian fits to these contiguous structures. In contrast Di Francesco et al. (2008) created the SCUBA Legacy Catalogue using Clumpfind which identifies irregular objects by following intensity contours. Due to this different approach in identification between the two catalogues the catalogued positions of IRDC cores and SCUBA clumps may differ by a considerable amount, even when the two are clearly morphologically associated with each other. A large positional matching radius was required to identify potential matches followed by further refinement by eye, checking that the individual IRDC cores were morphologically similar to the SCUBA $850 \mu\text{m}$ emission. A matching radius of $1'$ was chosen as Simon et al. (2006) quotes that typical core diameters lie between $0.75'$ and $2'$. For added confidence, those cores that were initially matched were additionally checked for $850 \mu\text{m}$ emission at the location of the MSX core.

On several occasions multiple matches were made to the same SCUBA sources where Clumpfind had only identified one object and vice versa. In these instances the closest positional Clumpfind match to the candidate MSX identified IRDC core was taken. A consequence of the differing techniques used to identify objects within the MSX and SCUBA catalogues was seen when classifying by eye those IRDC SCUBA detected candidates with and without embedded objects. Fig. 1, shows IRDC core MSXDGC028.37+00.07 (d), Clumpfind identified two distinct objects in the $850 \mu\text{m}$ data but the MSX identification process identified the dark complex as one object.

Of the 251 IRDC cores located within the SCUBA Legacy Catalogue mapped region a total of 46 core matches were manually excluded from the sample. In some cases, this was because the MSX identified IRDC cores were located on

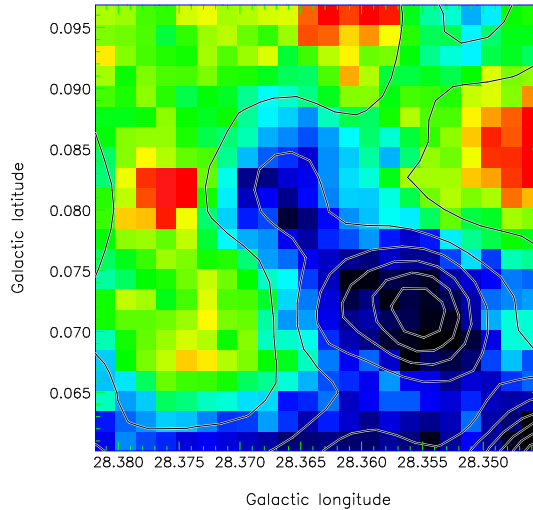


Figure 1. Image of IRDC core: MSXDGC028.37+00.07 (d). Image is MSX $8 \mu\text{m}$ with SCUBA contours overlaid.

positions of extended $850 \mu\text{m}$ emission which could not be morphologically matched to the compact candidate IRDC cores. Due to the large upper limit used for the matching radius a number of matches were also found to be inappropriate. In other cases, objects were found within $1'$ but not coincident with $850 \mu\text{m}$ emission. This may have occurred due to poor background modelling of the mid-infrared emission. The subtraction of a smoothed background model can potentially result in the creation of artifacts with high contrast values. Cores adjacent to bright extended $8 \mu\text{m}$ infrared emission, were also amongst those excluded. These objects were removed due to concerns over the process of creating a contrast image in a complex environment.

Finally of the 205 remaining IRDC cores, a total of 154 IRDC cores were matched to SCUBA objects from the SCUBA Legacy Catalogue of Di Francesco et al. (2008). The other remaining 51 IRDC cores were identified as having no corresponding $850 \mu\text{m}$ emission. These MSX identified candidate cores could be due to column densities and dust temperatures below the detection limit of SCUBA. Alternatively they could be a result of uncertainties in the MSX IRDC candidate identification process, we explore these possibilities further in section 4.2.

2.3 Column densities and masses of the cores

We derive peak column densities for all IRDC cores within our sample, whether detected at $850 \mu\text{m}$ or not, by applying the following extinction law to the MSX $8 \mu\text{m}$ data:

$$I_i = I_b e^{-\tau_\lambda} \quad (1)$$

where I_i is the image intensity, I_b is the background model intensity and τ_λ is the dust opacity which equals the cross sectional area, σ_λ , multiplied by the column density, $N(H_2)$, i.e. $\tau_\lambda = \sigma_\lambda \cdot N(H_2)$. The peak contrast value C is defined by Simon et al. (2006) as:

$$C = \frac{I_b - I_i}{I_b} = 1 - e^{-\tau_\lambda} \quad (2)$$

⁵ TOPCAT: Tool for OPERations on Catalogues And Tables. See <http://www.star.bris.ac.uk/~mbt/topcat/>

It is then possible, by substituting τ_λ from equation 1 into equation 2, to derive:

$$N(H_2) = \frac{-\ln(1-C)}{\sigma_\lambda} \quad (3)$$

We assume a value of $\sigma_\lambda = 2.3 \times 10^{-23} \text{ cm}^2$ for the cross sectional area of the obscuring dust particles at $8.8 \mu\text{m}$ (Ragan et al. 2006). Column densities for the IRDCs derived by this method are contained in Tables 1 and 2. Fig. 2 shows the distribution of those cores detected and not detected at $850 \mu\text{m}$ with peak contrast. We see that the median column density for the SCUBA detected candidates and the SCUBA non-detected candidates is $1.7 \times 10^{22} \text{ cm}^{-2}$ and $1.0 \times 10^{22} \text{ cm}^{-2}$ respectively.

For comparison with the values determined from the $8 \mu\text{m}$ extinction we also calculated the peak column densities for cores detected at $850 \mu\text{m}$, using the SCUBA $850 \mu\text{m}$ data to derive the mass (as defined by Hildebrand 1983) and assuming spherical geometry:

$$N(H_2) = \frac{F_\nu C_\nu}{B_\nu(T)\pi(\tan(B_{850}))^2 m_H} \quad (4)$$

where the mass coefficient C_ν is given by

$$C_\nu = \frac{M_g}{M_d \kappa_\nu} \quad (5)$$

F_ν is the observed peak flux; $B_\nu(T)$ is the Planck function evaluated for dust temperature, T ; B_{850} is the radius of the beam at $850 \mu\text{m}$, which has a FWHM of $19''$ due to convolution during the data reduction (Di Francesco et al. 2008) and m_H is the mass of a hydrogen atom. The value of $C_\nu = 50 \text{ g cm}^{-2}$ at $850 \mu\text{m}$ is taken from Kerton et al. (2001), where M_g is the gas mass and M_d is the dust mass and κ_ν is the dust opacity, assuming a gas to dust ratio of 100 and an opacity gradient β of 2.

When evaluating the Planck function, a temperature of 15 K was assumed for all the cores as this is the midpoint of the observed range (8–25 K) in IRDC temperatures observed by Carey et al. (1998), Teyssier et al. (2002) and Pillai et al. (2006). Decreasing or increasing the temperature to 8 or 25 K would increase or decrease these column density estimates by a factor of 3.5 and 2.2 respectively.

We compared the column densities derived by each method. In general the column density derived from the $8 \mu\text{m}$ extinction agrees with that derived from the $850 \mu\text{m}$ emission to within an order of magnitude. There is considerable scatter but the overall trend is that the $8 \mu\text{m}$ column density underestimates the $850 \mu\text{m}$ column density by roughly a factor of 2. This suggests that the average temperature for the IRDC cores may be closer to 10 K than our assumption of 15 K. However due to the large uncertainties in mass coefficients, the $8 \mu\text{m}$ extinction law and contamination from foreground emission we do not expect close agreement between these two methods.

Masses were determined for the cores detected at $850 \mu\text{m}$ using the method of Hildebrand (1983), i.e.

$$M = \frac{d^2 F_\nu C_\nu}{B_\nu(T)} \quad (6)$$

A dust temperature of 15 K was again assumed for all the cores. As before, decreasing or increasing the dust temperature to 8 or 25 K would increase or decrease the masses derived by a factor of 3.5 and 2.2 respectively. d is the distance

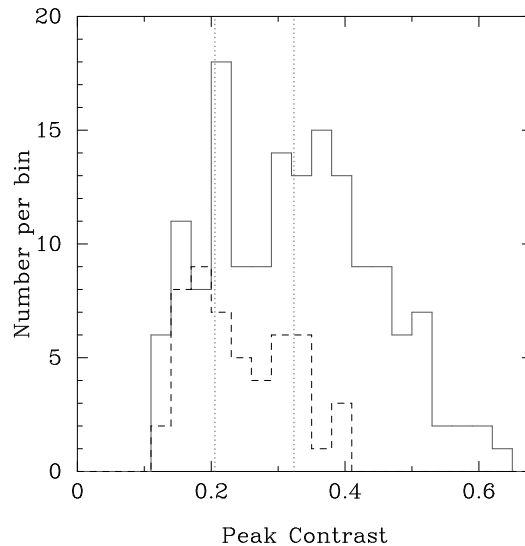


Figure 2. Histogram of Peak Contrast values for cores detected at $850 \mu\text{m}$ (solid line) and cores not detected at $850 \mu\text{m}$ (dashed line). Vertical lines mark the position of the peak contrast values that correspond to $1.7 \times 10^{22} \text{ cm}^{-2}$ and $1.0 \times 10^{22} \text{ cm}^{-2}$ (median column densities for cores detected and not detected at $850 \mu\text{m}$ respectively). Bin size used is 0.03.

to each core. Kinematic distances exist for 33 of our cores detected at $850 \mu\text{m}$ from Simon et al. (2006), who derived distances by matching up the morphologies of candidate IRDC cores with CO morphologies from the GRS (Galactic Ring Survey). Our mass estimates for these 33 SCUBA detected cores, along with the distance estimates from Simon et al. (2006) can be found in Table 3.

2.4 Embedded $24 \mu\text{m}$ objects in the cores

Of the 154 IRDC cores detected at $850 \mu\text{m}$, 69 were located within the coverage area of MIPS GAL and 34 out of the 51 cores not detected at $850 \mu\text{m}$ were also located within the MIPS GAL survey coverage area. The cores were visually inspected at $24 \mu\text{m}$ and it was found that 48 of the cores detected at $850 \mu\text{m}$ are positionally associated with one or more $24 \mu\text{m}$ MIPS GAL sources (approximately half contain more than one $24 \mu\text{m}$ source). None of the 34 cores not detected at $850 \mu\text{m}$ are found to be associated with any MIPS GAL $24 \mu\text{m}$ sources. Fig. 6 shows two cores that are seen at both $8 \mu\text{m}$ and $24 \mu\text{m}$, one with an embedded object and one without.

3 RESULTS

3.1 MSX identified IRDCs in the SCUBA Legacy Catalogue

In total 205 candidate IRDC MSX cores were found to be within the SCUBA Legacy Catalogue coverage area. 154 candidate cores had detectable emission at $850 \mu\text{m}$, and 51 candidate cores did not. Of the 154 cores detected at $850 \mu\text{m}$, we find that they span a range of peak contrast values (0.11–0.62), column densities and masses, with the peak contrast distribution having a median of 0.32. $8 \mu\text{m}$ column densities

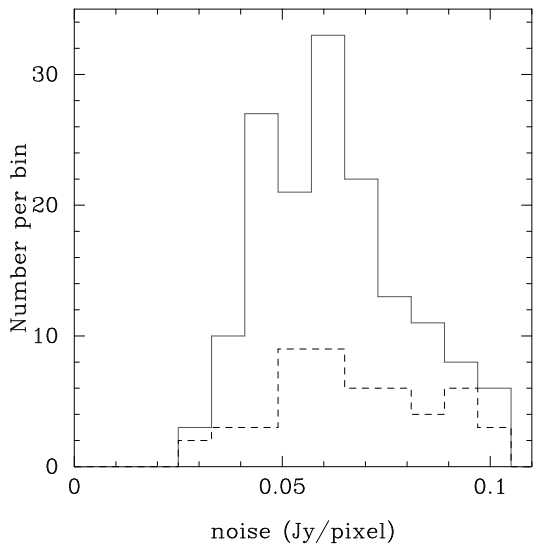


Figure 3. Histogram of rms (Jy/pixel) for cores detected at $850\ \mu\text{m}$ (solid line) and cores not detected at $850\ \mu\text{m}$ (dashed line). Bin size used is 0.008.

range from 0.56×10^{22} to $4.21 \times 10^{22}\ \text{cm}^{-2}$ with a median of $1.7 \times 10^{22}\ \text{cm}^{-2}$. Mass estimates of these candidates range from 50 to $4,190\ M_{\odot}$ with a median of $300\ M_{\odot}$. Peak contrast values for cores detected and not detected at $850\ \mu\text{m}$ are given in Tables 1 and 2 respectively. The physical properties of those cores with distance information available (data taken from Simon et al. (2006) and Jackson et al. (2008)) are seen in Table 3.

Those cores not detected at $850\ \mu\text{m}$ are found predominantly at low contrast values (≤ 0.4), with a mean of 0.22 (seen in Fig. 2). This result is not surprising, SCUBA is naturally expected to detect high column density clouds (which would have high contrast values) and not detect low column density clouds (which would have low contrast values). Although the cores not detected at $850\ \mu\text{m}$ possess lower peak contrasts, we see no evidence for the existence of two separate populations. A Kolmogorov-Smirnoff (KS) two sample test, on the peak contrast values for cores with and without $850\ \mu\text{m}$ emission, reveals no significant difference (to 95%) that the cores originate from two separate populations. Inspection of the rms values for the 205 candidate IRDC cores, as with the $850\ \mu\text{m}$ emission, reveals no significant difference in values between those cores detected at $850\ \mu\text{m}$ and those not detected at $850\ \mu\text{m}$ as seen in Fig. 3. Thus we are confident that the reason behind the cores not being detected at $850\ \mu\text{m}$ is not due to them simply lying in high noise regions of the SCUBA Legacy Catalogue. It is possible that some of the cores identified by Simon et al. (2006) that were not detected at $850\ \mu\text{m}$ are not true cores at all, rather voids in the mid-infrared background. This possibility is suggested by Simon et al. (2006) and Jackson et al. (2008), who state at low contrast values the number of mis-identified IRDCs is greater than at high contrasts.

3.2 Detection rates

We investigated the fraction of cores detected at $850\ \mu\text{m}$ versus peak contrast to identify any trends in the detection

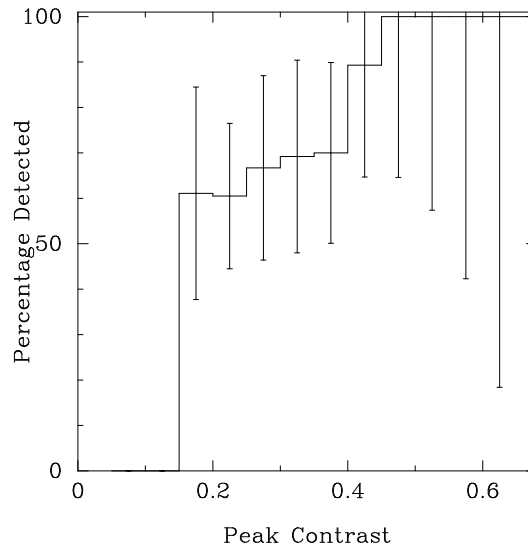


Figure 4. Histogram of contrast value against detection rate (defined as IRDC cores with associated $850\ \mu\text{m}$ sources). Bin size used is 0.05.

fraction of IRDC cores. We calculated the detection fraction by dividing the number of cores with $850\ \mu\text{m}$ detections by the total number of MSX IRDC cores within the SCUBA Legacy Catalogue at specific contrast values. Overall the fraction of IRDC cores detected by SCUBA is found to be 75%. At low contrast values we detect over 60% of the IRDC cores, whereas all IRDC cores are detected when the contrast is high as seen in Fig. 4. The error bars in Fig. 4 were calculated by assuming an uncertainty of \sqrt{N} where N is the number of cores detected by SCUBA per bin and using propagation of errors.

3.3 MIPS GAL $24\ \mu\text{m}$ sources associated with IRDCs detected at $850\ \mu\text{m}$

We present a histogram of the 69 IRDC cores detected at $850\ \mu\text{m}$ within the MIPS GAL coverage area in Fig. 5. 48 of the IRDC cores were found to be positionally associated with one or more $24\ \mu\text{m}$ MIPS GAL sources and 21 were found not to be associated with any MIPS GAL sources

To investigate if the cores with and without embedded $24\ \mu\text{m}$ objects were drawn from the same population, a KS test was once again performed on their peak contrast distribution and it was found that they are highly likely to originate from the same population, with no distinct differences in their peak contrast distribution to a level of significance $> 99\%$.

4 DISCUSSION

4.1 The reliability of the MSX IRDC catalogue

Originally, when the Simon et al. (2006) catalogue was published, an initial reliability of 82% was reported for IRDCs with contrast values > 0.25 . This initial reliability was estimated for the large high contrast clouds by comparison to other source lists from MSX and ISO data (Simon et al.

Table 1. Data for all MSX identified IRDC candidate cores within the SCUBA Legacy Catalogue, with a SCUBA detection. C is the Peak contrast value. F_{850} is the peak flux at 850 μm .

MSX ID (MSXDC)	SCUBA ID (JCMTS ^b)	RA (hh:mm:ss)	Dec ($^{\circ}$: $'$: $''$)	C	F_{850} (Jy/beam)	$N_8(\text{H}_2)$ $\times 10^{22}$ (cm^{-2})	$N_{850}(\text{H}_2)$ $\times 10^{22}$ (cm^{-2})	MIPS source ^a
G000.06+00.21 (a)	F_J174457.0-284618	17:44:55.4	-28:46:38	0.22	1.09	1.08	7.91	
G000.07+00.24 (a)	F_J174450.2-284449	17:44:50.7	-28:44:45	0.16	0.40	0.76	2.89	
G000.08+00.19 (a)	F_J174503.4-284618	17:45:03.8	-28:46:09	0.15	0.76	0.77	5.51	
G000.13-00.14 (a)	F_J174626.0-285437	17:46:26.8	-28:54:38	0.22	1.41	1.08	10.22	
G000.20-00.25 (a)	F_J174706.6-285314	17:47:06.3	-28:53:26	0.19	0.57	0.92	4.13	
G000.21+00.23 (a)	F_J174510.6-283812	17:45:13.8	-28:37:59	0.14	0.59	0.66	4.28	
G000.25+00.02 (a)	F_J174607.0-284130	17:46:07.9	-28:41:35	0.44	6.62	2.52	47.95	
G000.32-00.23 (a)	F_J174719.9-284656	17:47:19.3	-28:47:01	0.26	0.73	1.31	5.29	
G000.32-00.18 (a)	F_J174707.2-284432	17:47:08.6	-28:45:19	0.33	0.46	1.74	3.33	
G000.33+00.05 (a)	F_J174613.0-283654	17:46:12.7	-28:37:10	0.21	3.74	1.02	27.21	
G000.35-00.24 (a)	F_J174725.4-284538	17:47:23.3	-28:45:47	0.16	0.34	0.76	2.46	
G000.40-00.21 (a)	F_J174725.4-284156	17:47:25.3	-28:42:16	0.23	1.26	1.14	9.14	
G000.40+00.04 (a)	F_J174624.4-283331	17:46:24.7	-28:33:47	0.45	6.76	2.60	49.03	
G000.59+00.01 (e)	F_J174646.8-283155	17:46:47.5	-28:32:07	0.37	14.95	2.01	112.31	
G000.59+00.01 (a)	F_J174643.2-283007	17:46:42.9	-28:30:27	0.47	7.83	2.76	56.80	
G000.59+00.01 (c)	F_J174648.6-282944	17:46:49.2	-28:29:53	0.37	2.71	2.01	19.65	
G000.59+00.01 (f)	F_J174653.2-282632	17:46:53.0	-28:26:40	0.34	2.18	1.81	15.81	
G000.59+00.01 (d)	F_J174657.8-282332	17:46:59.7	-28:23:06	0.37	2.10	2.01	16.20	
G000.59+00.01 (b)	F_J174709.6-282208	17:47:09.3	-28:21:54	0.37	3.38	2.01	24.41	
G000.68-00.18 (a)	F_J174800.1-282714	17:48:01.2	-28:27:24	0.20	0.67	0.97	4.86	
G000.72-00.08 (a)	F_J174740.1-282132	17:47:39.0	-28:21:39	0.16	3.49	0.76	25.27	
G000.87-00.01 (a)	E_J174744.6-281150	17:47:45.4	-28:11:47	0.15	1.91	0.77	13.84	
G000.90-00.02 (a)	E_J174751.4-281039	17:47:51.1	-28:10:46	0.13	1.87	0.61	13.56	
G000.94+00.00 (a)	E_J174750.1-280803	17:47:49.5	-28:07:37	0.17	1.13	0.81	8.19	
G000.97+00.04 (a)	E_J174744.6-280445	17:47:45.3	-28:04:45	0.22	1.18	1.08	8.55	
G000.98+00.09 (a)	E_J174733.3-280302	17:47:32.7	-28:02:30	0.13	0.86	0.61	6.24	
G000.97-00.06 (c)	E_J174831.4-280826	17:48:30.3	-28:08:25	0.22	1.39	1.08	10.09	
G001.01+00.05 (b)	E_J174752.3-280321	17:47:53.0	-28:03:27	0.20	0.92	0.97	8.42	
G000.97-00.06 (a)	E_J174814.6-280550	17:48:15.3	-28:06:05	0.26	1.55	1.31	11.23	
G001.01+00.05 (a)	E_J174747.8-280157	17:47:49.1	-28:01:58	0.20	0.90	0.97	6.52	
G001.02+00.02 (a)	E_J174755.5-280239	17:47:57.0	-28:02:48	0.11	0.67	0.57	4.86	
G001.11-00.16 (a)	F_J174846.7-280338	17:48:47.9	-28:03:28	0.29	1.30	1.49	9.42	
G001.11-00.16 (b)	F_J174851.3-280356	17:48:52.4	-28:04:01	0.24	0.59	1.19	4.28	
G001.13-00.26 (a)	F_J174915.8-280531	17:49:16.5	-28:05:39	0.20	0.71	0.97	5.14	
G001.26-00.23 (a)	F_J174930.3-275848	17:49:31.4	-27:59:01	0.14	0.36	0.66	2.61	
G001.26+00.04 (a)	F_J174826.6-274949	17:48:25.3	-27:49:53	0.21	1.78	1.02	12.89	
G001.29+00.03 (a)	F_J174833.4-274836	17:48:32.5	-27:48:45	0.17	1.62	0.81	11.75	
G001.31-00.04 (a)	F_J174856.9-275047	17:48:57.0	-27:50:28	0.17	0.67	0.81	4.86	
G001.34-00.08 (a)	F_J174906.9-274946	17:49:06.7	-27:49:48	0.13	0.42	0.61	3.05	
G001.47-00.03 (a)	F_J174914.3-274211	17:49:13.2	-27:41:55	0.18	0.40	0.86	2.89	
G001.46+00.03 (a)	E_J174855.8-273917	17:48:56.3	-27:39:24	0.29	2.31	1.49	16.74	
G001.51-00.10 (a)	F_J174934.7-274212	17:49:36.7	-27:41:53	0.17	1.64	0.81	11.88	
G001.53+00.14 (a)	E_J174842.2-273230	17:48:41.0	-27:33:04	0.13	0.82	0.61	5.94	
G001.61-00.02 (b)	E_J174936.6-273248	17:49:36.5	-27:33:11	0.37	0.71	2.01	5.14	
G001.61-00.02 (a)	E_J174944.3-273330	17:49:44.4	-27:33:11	0.41	2.67	2.29	19.35	
G001.67-00.18 (b)	E_J175015.0-273437	17:50:16.0	-27:34:22	0.23	0.63	1.14	4.56	
G002.51+00.18 (b)	F_J175045.8-263945	17:50:43.4	-26:40:21	0.38	2.77	2.08	20.09	
G002.51+00.18 (a)	F_J175045.8-263945	17:50:48.5	-26:39:30	0.41	2.77	2.29	20.09	
G008.83-00.05 (e)	F_J180525.3-211926	18:05:27.7	-21:20:17	0.27	4.22	1.37	30.67	
G008.83-00.05 (a)	F_J180525.3-211926	18:05:26.3	-21:19:04	0.32	4.22	1.68	30.67	
G009.84-00.03 (a)	E_J180733.9-202613	18:07:37.4	-20:26:20	0.43	0.65	2.44	4.71	yes
G010.71-00.16 (g)	E_J180944.4-194712	18:09:44.4	-19:47:02	0.35	0.46	1.87	3.33	yes
G010.71-00.16 (h)	E_J180953.3-194806	18:09:52.5	-19:47:40	0.34	0.65	1.81	4.71	yes

^a cores with MIPS data available are denoted by a yes (if an embedded 24 μm source is present) or no (if an embedded 24 μm is not present) in this column^b F stands for Fundamental catalogue and E stands for Extended catalogue

Table 1. - Continued

MSX ID (MSXDC)	SCUBA ID (JCMTS)	RA (hh:mm:ss)	Dec (°:':")	C	F ₈₅₀ (Jy/beam)	N ₈ (H ₂) ×10 ²² (cm ⁻²)	N ₈₅₀ (H ₂) ×10 ²² (cm ⁻²)	MIPS source
G010.71-00.16 (b)	E_J180938.7-194512	18:09:38.7	-19:45:15	0.49	2.79	2.93	20.22	yes
G010.71-00.16 (d)	E_J180949.1-194442	18:09:48.9	-19:44:52	0.40	0.44	2.22	3.20	no
G010.71-00.16 (f)	E_J180940.8-194336	18:09:41.5	-19:43:42	0.36	2.35	1.94	17.04	no
G010.71-00.16 (a)	E_J180945.7-194206	18:09:45.5	-19:42:22	0.56	1.28	3.57	9.29	yes
G010.71-00.16 (e)	E_J181009.0-194507	18:10:10.0	-19:45:13	0.38	0.63	2.80	4.56	no
G010.71-00.16 (c)	E_J181003.1-194342	18:10:02.4	-19:43:28	0.44	0.84	2.52	6.09	yes
G010.99-00.07 (a)	F_J181007.1-192755	18:10:07.2	-19:27:60	0.55	1.39	3.47	10.09	yes
G011.11-00.11 (g)	F_J181013.5-192419	18:10:13.7	-19:24:36	0.30	0.67	1.55	4.86	no
G011.11-00.11 (b)	F_J181018.2-192431	18:10:18.7	-19:24:42	0.43	0.88	2.44	6.37	yes
G011.11-00.11 (a)	F_J181033.0-192201	18:10:32.0	-19:22:31	0.50	1.45	3.01	10.52	yes
G011.11-00.11 (f)	F_J181033.0-192201	18:10:35.4	-19:21:02	0.30	0.73	1.55	5.29	yes
G011.11-00.11 (d)	F_J181037.3-191820	18:10:37.7	-19:18:27	0.31	0.36	1.61	2.61	yes
G011.11-00.11 (c)	F_J181034.8-191702	18:10:35.3	-19:17:20	0.40	0.80	2.22	5.81	yes
G011.11-00.11 (e)	F_J181039.9-191132	18:10:40.6	-19:10:58	0.31	0.76	1.61	5.51	yes
G012.44-00.14 (b)	F_J181320.6-181220	18:13:21.6	-18:12:17	0.34	0.36	1.81	2.61	yes
G012.44-00.14 (a)	F_J181341.7-181239	18:13:41.5	-18:12:32	0.45	1.43	2.60	20.37	yes
G012.44-00.14 (d)	F_J181331.6-181115	18:13:32.5	-18:11:18	0.29	0.36	1.49	2.61	no
G012.88+00.53 (a)	F_J181145.3-173044	18:11:44.8	-17:31:17	0.36	1.11	1.94	8.06	yes
G013.02-00.83 (a)	F_J181700.1-180202	18:17:00.7	-18:02:18	0.47	0.27	2.76	1.97	yes
G013.68-00.60 (a)	F_J181725.7-172049	18:17:27.6	-17:20:59	0.24	0.42	1.19	3.05	no
G018.50-00.16 (c)	E_J182517.5-125526	18:25:17.5	-12:55:31	0.27	0.29	1.37	2.10	no
G018.50-00.16 (d)	F_J182523.2-125450	18:25:23.3	-12:54:55	0.25	0.59	1.25	4.28	no
G018.50-00.16 (b)	F_J182520.4-125014	18:25:21.2	-12:50:18	0.29	0.32	1.49	2.31	no
G018.58-00.08 (b)	F_J182507.3-124750	18:25:07.6	-12:48:00	0.32	0.46	1.68	3.33	yes
G018.58-00.08 (a)	F_J182508.5-124520	18:25:08.9	-12:45:20	0.37	1.91	2.01	13.84	yes
G019.27+00.07 (a)	F_J182552.1-120456	18:25:54.0	-12:04:56	0.50	1.03	3.01	7.47	yes
G022.35+00.41 (b)	F_J183029.6-091238	18:30:28.7	-09:12:31	0.37	0.38	2.01	2.76	no
G022.35+00.41 (a)	F_J183024.4-091038	18:30:24.7	-09:10:47	0.51	1.89	3.10	13.69	yes
G023.86-00.19 (a)	E_J183526.9-080814	18:35:26.6	-08:08:22	0.32	0.42	1.68	3.05	no
G024.00+00.15 (a)	E_J183428.8-075220	18:34:29.5	-07:52:23	0.20	1.11	0.97	8.06	yes
G024.36-00.16 (a)	F_J183618.3-074102	18:36:17.5	-07:41:27	0.41	0.88	2.29	6.37	yes
G024.37-00.21 (a)	F_J183630.0-074208	18:36:30.2	-07:42:16	0.34	0.34	1.81	2.46	yes
G024.60+00.08 (a)	F_J183540.1-071838	18:35:39.4	-07:18:51	0.49	2.02	2.93	14.64	yes
G024.68+00.17 (a)	F_J183540.1-071514	18:35:41.2	-07:15:22	0.20	0.25	0.97	1.81	yes
G025.04-00.20 (g)	F_J183712.0-071126	18:37:12.8	-07:11:23	0.36	0.76	1.94	5.51	yes
G025.04-00.20 (e)	F_J183719.2-071144	18:37:18.8	-07:11:49	0.41	1.13	2.29	8.19	yes
G025.04-00.20 (b)	F_J183734.6-070726	18:37:34.8	-07:07:39	0.44	0.38	2.52	2.76	yes
G025.04-00.20 (f)	F_J183738.2-070550	18:37:38.2	-07:06:00	0.38	0.29	2.08	2.10	no
G028.37+00.07 (a)	F_J184250.6-040314	18:42:50.6	-04:03:30	0.61	2.52	4.09	18.27	yes
G028.37+00.07 (d)	F_J184248.2-040133	18:42:48.6	-04:01:42	0.47	0.65	2.76	4.71	yes
G028.37+00.07 (b)	F_J184255.4-040150	18:42:55.5	-04:01:47	0.51	0.95	3.10	6.89	no
G028.37+00.07 (e)	F_J184300.2-040132	18:43:00.5	-04:01:36	0.45	0.69	2.60	5.01	no
G028.53-00.25 (g)	F_J184417.3-040208	18:44:17.0	-04:02:18	0.27	0.61	1.37	5.40	yes
G028.53-00.25 (b)	F_J184422.5-040150	18:44:23.7	-04:02:09	0.38	0.57	2.08	4.13	yes
G028.53-00.25 (c)	F_J184415.6-040056	18:44:16.6	-04:01:02	0.34	1.03	1.81	7.47	yes
G028.53-00.25 (a)	F_J184418.1-035938	18:44:17.1	-03:59:37	0.41	2.65	2.29	19.20	yes
G028.53-00.25 (e)	F_J184418.1-035938	18:44:17.7	-03:58:16	0.29	0.69	1.49	5.01	yes
G028.61-00.26 (a)	F_J184428.1-035750	18:44:29.0	-03:57:46	0.27	0.32	1.37	2.31	yes
G030.77+00.22 (a)	F_J184647.8-014856	18:46:47.1	-01:49:03	0.25	4.62	1.25	33.48	yes
G030.97-00.14 (a)	E_J184821.9-014832	18:48:24.2	-01:48:25	0.38	1.89	2.08	13.69	yes
G031.03+00.26 (b)	F_J184701.4-013438	18:47:01.5	-01:34:47	0.29	0.78	1.49	5.66	yes
G031.03+00.26 (c)	F_J184707.4-013432	18:47:07.7	-01:34:42	0.29	0.50	1.49	3.63	yes
G031.03+00.26 (a)	F_J184701.4-013314	18:47:01.2	-01:33:23	0.31	0.55	1.61	4.00	yes
G031.23+00.05 (a)	E_J184807.5-012844	18:48:08.3	-01:28:50	0.21	0.82	1.02	5.94	yes
G031.27+00.08 (a)	E_J184807.9-012626	18:48:08.0	-01:26:43	0.16	0.69	0.76	5.01	no
G031.38+00.29 (a)	F_J184732.6-011338	18:47:34.0	-01:13:59	0.38	1.53	2.08	11.10	no
G031.97+00.07 (b)	F_J184922.1-005038	18:49:22.2	-00:50:47	0.42	0.59	2.37	4.28	yes
G031.97+00.07 (c)	F_J184926.9-005002	18:49:27.0	-00:50:11	0.35	0.36	1.87	2.61	no
G033.69-00.01 (e)	E_J185248.6+003602	18:52:49.6	+00:35:55	0.32	0.63	1.68	4.56	no
G033.69-00.01 (b)	E_J185252.6+003832	18:52:53.1	+00:38:10	0.38	0.65	2.08	4.71	no
G033.69-00.01 (c)	E_J185253.8+004120	18:52:53.0	+00:40:44	0.37	0.59	2.01	4.28	no

Table 1. - Continued

MSX ID (MSXDC)	SCUBA ID (JCMTS)	RA (hh:mm:ss)	Dec (°: ': ")	C	F ₈₅₀ (Jy/beam)	N ₈ (H ₂) ×10 ²² (cm ⁻²)	N ₈₅₀ (H ₂) ×10 ²² (cm ⁻²)	MIPS source
G033.69−00.01 (a)	E_J185257.0+004302	18:52:57.6	+00:42:59	0.38	1.60	2.08	11.60	yes
G034.43+00.24 (a)	F_J185318.9+012650	18:53:18.9	+01:26:39	0.34	0.38	1.81	2.76	yes
G038.95−00.47 (a)	F_J190407.5+050844	19:04:08.3	+05:08:49	0.53	1.37	3.28	9.94	yes
G048.52−00.47 (a)	F_J192207.4+133713	19:22:07.9	+13:36:58	0.38	0.29	2.08	2.10	no
G048.65−00.29 (a)	F_J192144.7+134925	19:21:45.3	+13:49:22	0.34	0.40	1.81	2.89	yes
G079.24+00.41 (b)	E_J203137.7+401935	20:31:38.1	+40:19:38	0.51	0.88	3.10	6.37	
G079.24+00.41 (a)	F_J203157.6+401828	20:31:56.8	+40:18:12	0.52	1.99	3.19	14.43	
G081.67+00.44 (a)	F_J203924.9+421555	20:39:21.0	+42:15:47	0.23	2.31	1.14	16.74	
G081.73+00.59 (a)	F_J203859.3+422330	20:38:58.2	+42:23:55	0.27	8.19	1.37	59.39	
G081.76+00.63 (a)	F_J203851.6+422717	20:38:52.6	+42:27:12	0.17	0.80	0.81	5.81	
G351.52+00.69 (a)	F_J172056.6-354044	17:20:58.2	-35:40:28	0.39	2.48	2.15	17.97	
G353.26−00.16 (a)	F_J172935.1-344316	17:29:33.6	-34:43:31	0.31	0.44	1.61	3.20	
G353.37−00.33 (b)	F_J173012.1-344328	17:30:12.4	-34:43:45	0.38	1.47	2.08	10.65	
G353.37−00.33 (a)	F_J173017.0-344217	17:30:18.8	-34:41:58	0.43	2.29	2.44	19.61	
G353.90+00.25 (e)	F_J172902.5-335950	17:29:02.2	-34:00:12	0.46	1.13	2.68	8.19	
G353.90+00.25 (a)	F_J172917.1-340017	17:29:12.8	-34:00:01	0.62	0.55	4.21	4.00	
G353.90+00.25 (f)	F_J172917.1-340017	17:29:16.8	-34:00:25	0.46	0.61	2.68	5.40	
G353.90+00.25 (c)	F_J172919.4-335550	17:29:19.1	-33:55:59	0.50	0.59	3.01	4.28	
G353.90+00.25 (b)	F_J172928.5-335444	17:29:27.9	-33:55:06	0.59	0.50	3.88	3.63	
G353.90+00.25 (d)	F_J172927.1-335302	17:29:25.0	-33:53:03	0.49	0.90	2.93	6.52	
G359.05+00.00 (a)	F_J174321.6-294437	17:43:21.8	-29:44:43	0.27	0.63	1.37	4.56	
G359.06−00.03 (a)	F_J174326.7-294531	17:43:29.7	-29:45:22	0.16	0.71	0.76	5.14	
G359.08+00.04 (a)	F_J174314.8-294143	17:43:14.8	-29:42:02	0.20	0.50	0.97	3.63	
G359.29−00.03 (a)	F_J174404.5-293302	17:44:03.5	-29:33:12	0.21	1.28	1.02	9.29	
G359.37−00.28 (a)	F_J174514.5-293644	17:45:14.1	-29:37:27	0.12	0.27	0.56	19.57	
G359.41+00.08 (a)	F_J174354.0-292314	17:43:53.9	-29:23:27	0.16	1.03	0.76	7.47	
G359.46−00.03 (a)	F_J174428.9-292426	17:44:29.3	-29:24:18	0.28	2.42	1.43	19.54	
G359.48−00.22 (a)	F_J174514.4-292902	17:45:15.1	-29:29:30	0.14	1.87	0.66	13.56	
G359.59+00.02 (a)	F_J174436.3-291621	17:45:33.5	-29:24:26	0.31	1.87	1.61	15.56	
G359.60−00.22 (b)	F_J174535.0-292456	17:44:32.0	-29:16:05	0.20	1.97	0.97	14.28	
G359.60−00.22 (a)	F_J174535.0-292314	17:45:35.2	-29:23:15	0.36	5.50	1.94	39.96	
G359.68−00.13 (a)	F_J174526.3-291608	17:45:25.3	-29:16:06	0.20	0.61	0.97	5.40	
G359.80−00.13 (a)	F_J174539.0-291132	17:45:37.1	-29:11:25	0.32	1.62	1.68	11.75	
G359.82+00.12 (a)	F_J174443.6-290127	17:44:43.1	-29:01:02	0.19	0.44	0.92	3.20	
G359.83+00.18 (a)	E_J174429.3-285901	17:44:29.5	-28:59:13	0.21	0.38	1.02	2.76	
G359.85+00.21 (a)	E_J174425.2-285643	17:44:25.3	-28:56:49	0.23	0.38	1.14	2.76	
G359.87−00.09 (a)	F_J174544.0-290502	17:45:43.4	-29:05:22	0.25	5.44	1.25	3.95	
G359.90−00.30 (a)	F_J174636.3-291011	17:46:35.8	-29:10:26	0.35	2.33	1.87	16.89	
G359.91+00.17 (b)	F_J174444.4-285519	17:44:43.6	-28:55:28	0.45	0.90	2.60	6.52	
G359.91+00.17 (a)	F_J174448.5-285349	17:44:47.6	-28:53:54	0.58	4.41	3.77	31.96	

2006 and references there in). Later Jackson et al. (2008) determined a reliability (against CS J=2−1 detections) for low contrast (0.2-0.4) objects of approximately 50% increasing to almost 100% at high contrasts (>0.6), with an overall reliability of ~59%. However the Jackson et al. (2008) sample lacked very low contrast objects, the selection criteria used were peak contrasts >0.32 and angular sizes >42". Expanding this estimate to the whole MSX IRDC catalogue Jackson et al. (2008) stated that it was >50% reliable for all contrasts. These estimates of reliability were obtained via molecular line spectroscopy of ¹³CO and CS data from Simon et al. (2006) and Jackson et al. (2008) respectively.

Our mean detection rate of IRDC cores with 850 μm emission is 75% (this value varies over a range of peak contrast values as seen in Fig. 4) which is greater than the reliability of 50% stated by Jackson et al. (2008). However this

detection rate does not take into account the number of inconclusive matches that make up 19% of the IRDC sample. The close correspondence of 850 μm emission, CS 2−1 and ¹³CO detection rates for IRDCs places greater confidence in the high contrast Simon et al. (2006) candidate IRDCs as true molecular clouds.

4.2 Cores not detected at 850 μm

Of the 205 cores within our sample 51 cores were not detected at 850 μm. Those cores detected at 850 μm were found to have higher peak contrast values and column densities than those cores not detected at 850 μm. The difference in peak contrast values can be seen in Fig. 2. The median column density of the cores detected at 850 μm is a factor of ~1.6 times greater than the cores not detected at 850 μm. A KS

Table 2. Data for all MSX identified IRDC candidate cores within the SCUBA Legacy Catalogue, with no detection at 850 μm .

MSX ID (MSXDC)	l ($^{\circ}$)	b ($^{\circ}$)	RA (hh:mm:ss)	Dec ($^{\circ}$:':")	Peak Contrast	$N_S(\text{H}_2)$ $\times 10^{22} \text{ cm}^{-2}$
G000.13–00.14 (b)	0.163	-0.164	17:46:38.8	-28:52:56	0.19	0.92
G000.13–00.19 (a)	0.131	-0.196	17:46:41.8	-28:55:34	0.21	1.02
G000.36–00.21 (a)	0.364	-0.216	17:47:19.6	-28:44:14	0.20	0.97
G000.73–00.01 (a)	0.733	-0.014	17:47:24.6	-28:19:02	0.15	0.77
G001.62–00.08 (a)	1.631	-0.092	17:49:48.6	-27:35:17	0.16	0.76
G004.33–00.04 (a)	4.336	-0.052	17:55:48.0	-25:14:19	0.34	1.81
G004.33–00.04 (c)	4.358	-0.056	17:55:51.9	-25:13:18	0.29	1.49
G006.06–01.39 (a)	6.063	-1.397	18:04:43.5	-24:24:28	0.23	1.14
G006.09–01.39 (a)	6.094	-1.396	18:04:47.3	-24:22:49	0.24	1.19
G006.09–01.36 (a)	6.094	-1.367	18:04:40.6	-24:21:58	0.20	0.97
G010.57–00.30 (a)	10.588	-0.311	18:10:08.1	-19:55:35	0.33	1.74
G010.94–00.05 (a)	10.944	-0.059	18:09:55.7	-19:29:35	0.18	0.86
G012.37+00.50 (c)	12.431	0.496	18:10:54.4	-17:55:22	0.29	1.49
G012.44–00.20 (a)	12.449	-0.201	18:13:30.9	-18:14:31	0.15	0.77
G012.88+00.53 (c)	12.886	0.528	18:11:42.5	-17:30:31	0.29	1.49
G013.15+00.09 (a)	13.154	0.099	18:13:49.6	-17:28:46	0.25	1.25
G017.00+00.67 (a)	17.003	0.661	18:19:22.5	-13:49:34	0.33	1.74
G017.01+00.78 (a)	17.013	0.789	18:18:55.8	-13:45:24	0.13	0.61
G017.03+00.71 (a)	17.029	0.719	18:19:13.0	-13:46:33	0.14	0.66
G017.10+00.71 (a)	17.096	0.699	18:19:25.1	-13:43:34	0.31	1.61
G017.10+00.71 (b)	17.129	0.711	18:19:26.4	-13:41:29	0.31	1.61
G018.99–00.30 (b)	19.004	-0.306	18:26:44.4	-12:30:45	0.28	1.43
G024.60+00.08 (b)	24.659	0.163	18:35:40.9	-07:16:57	0.32	1.68
G024.60+00.08 (d)	24.596	0.131	18:35:40.7	-07:21:11	0.29	1.49
G025.12–00.16 (a)	25.126	-0.162	18:37:42.6	-07:01:01	0.12	0.56
G025.37–00.06 (a)	25.419	-0.104	18:38:02.7	-06:43:48	0.26	1.31
G025.42+00.10 (a)	25.426	0.109	18:37:17.7	-06:37:34	0.14	0.66
G027.93–00.34 (a)	27.924	-0.344	18:43:30.8	-04:36:47	0.19	0.92
G031.32+00.09 (a)	31.326	0.094	18:48:10.4	-01:23:11	0.17	0.81
G031.33+00.12 (a)	31.336	0.124	18:48:05.1	-01:21:49	0.16	0.76
G033.69–00.01 (d)	33.639	-0.056	18:52:55.6	+00:36:14	0.35	1.87
G034.94+00.37 (a)	34.941	0.384	18:53:44.2	+01:57:47	0.18	0.86
G042.75+00.01 (a)	42.751	0.019	19:09:25.2	+08:44:19	0.21	1.02
G042.75–00.19 (a)	42.753	-0.202	19:10:13.0	+08:38:18	0.22	1.08
G080.88–00.12 (a)	80.886	-0.131	20:39:16.7	+41:17:23	0.21	1.02
G081.49+00.13 (a)	81.504	0.129	20:40:11.5	+41:56:17	0.40	2.22
G081.49+00.13 (b)	81.498	0.161	20:40:02.2	+41:57:11	0.34	1.81
G081.56+00.57 (a)	81.564	0.581	20:38:27.4	+42:15:40	0.16	0.76
G081.57+00.50 (b)	81.576	0.523	20:38:44.7	+42:14:07	0.27	1.37
G081.60+00.58 (a)	81.603	0.586	20:38:33.7	+42:17:42	0.17	0.81
G081.69+00.71 (a)	81.699	0.708	20:38:21.2	+42:26:43	0.19	0.92
G351.50+00.66 (a)	351.509	0.661	17:21:05.1	-35:41:56	0.17	0.81
G353.26–00.16 (f)	353.281	-0.207	17:29:28.1	-34:43:09	0.24	1.19
G353.90+00.25 (g)	353.886	0.254	17:29:13.6	-33:57:36	0.40	2.22
G353.98+00.39 (a)	353.993	0.391	17:28:57.7	-33:47:43	0.20	0.97
G359.25+00.01 (a)	359.254	0.016	17:43:46.2	-29:33:50	0.15	0.77
G359.28+00.02 (a)	359.298	0.031	17:43:49.0	-29:31:06	0.38	2.08
G359.28+00.02 (b)	359.298	0.006	17:43:54.9	-29:31:54	0.34	1.81
G359.79–00.25 (b)	359.799	-0.267	17:46:11.1	-29:14:48	0.23	1.14
G359.81–00.29 (a)	359.814	-0.297	17:46:20.3	-29:14:58	0.17	0.81
G359.82–00.37 (b)	359.843	-0.367	17:46:40.9	-29:15:40	0.27	1.37

test of the peak contrast distribution could find no significant difference between the cores detected at 850 μm and those that were not.

Although the mid-infrared contrast value for a particular cloud should vary with the intensity of the background, it is possible to determine an estimate of the peak contrast sensitivity of SCUBA as a function of temperature by sub-

stituting equation 3 into equation 4, using an 850 μm flux limit of 3σ (where σ is the median rms sensitivity of the SCUBA Legacy Catalogue) for F_ν and rearranging for C :

$$C = 1 - \exp\left(-\frac{F_\nu C_\nu \sigma_\lambda}{B_\nu(T)\pi(\tan(B_{850}))^2 m_H}\right) \quad (7)$$

The median rms sensitivity value at 850 μm in the

Table 3. Mass estimates for clouds with distances obtained by the GRS survey (Jackson et al. 2008). Galactic coordinates quoted come from the MSX catalogue positions (Simon et al. 2006).

MSX ID (MSXDC)	SCUBA ID (JCMTS)	l ($^{\circ}$)	b ($^{\circ}$)	Peak Contrast	Flux ^a Jy	Distance kpc	Mass M_{\odot}	MIPS detected?
G018.50–00.16 (b)	F_J182520.4-125014	18.558	-0.159	0.29	1.79	4.1	240	No
G018.58–00.08 (b)	F_J182507.3-124750	18.566	-0.092	0.32	0.97	3.8	110	Yes
G018.58–00.08 (a)	F_J182508.5-124520	18.608	-0.076	0.37	4.51	3.8	500	Yes
G019.27+00.07 (a)	F_J182552.1-120456	19.289	0.076	0.50	3.24	2.4	130	Yes
G022.35+00.41 (b)	F_J183029.6-091238	22.356	0.416	0.37	2.02	4.3	290	No
G022.35+00.41 (a)	F_J183024.4-091038	22.374	0.444	0.51	4.94	4.3	720	Yes
G023.86–00.19 (a)	E_J183526.9-080814	23.871	-0.179	0.32	1.92	4.0	240	No
G024.36–00.16 (a)	F_J183618.3-074102	24.366	-0.159	0.41	1.77	3.9	190	Yes
G024.37–00.21 (a)	F_J183630.0-074208	24.378	-0.212	0.34	0.46	3.9	50	Yes
G024.60+00.08 (a)	F_J183540.1-071838	24.628	0.154	0.49	5.22	3.7	560	Yes
G028.37+00.07 (a)	F_J184250.6-040314	28.341	0.058	0.61	10.8	5.0	1010	Yes
G028.37+00.07 (d)	F_J184248.2-040133	28.364	0.079	0.47	2.52	5.0	100	Yes
G028.37+00.07 (g)	F_J184239.7-040027	28.366	0.121	0.38	1.36	5.0	100	No
G028.37+00.07 (b)	F_J184255.4-040150	28.376	0.053	0.51	3.34	5.0	310	No
G028.37+00.07 (e)	F_J184300.2-040132	28.388	0.036	0.45	2.18	5.0	130	No
G028.37+00.07 (f)	F_J184252.3-035956	28.403	0.064	0.43	3.72	5.0	4160	No
G028.53–00.25 (a)	F_J184418.1-035938	28.563	-0.232	0.41	12.8	5.7	4190	Yes
G028.61–00.26 (a)	F_J184428.1-035750	28.613	-0.262	0.27	0.56	4.2	80	Yes
G030.97–00.14 (a)	E_J184821.9-014832	30.978	-0.149	0.38	6.30	5.1	1270	Yes
G031.03+00.26 (b)	F_J184701.4-013438	31.023	0.261	0.29	2.97	6.6	520	Yes
G031.03+00.26 (c)	F_J184707.4-013432	31.036	0.239	0.29	1.32	6.6	160	Yes
G031.03+00.26 (a)	F_J184701.4-013314	31.043	0.273	0.31	3.43	6.6	460	Yes
G031.38+00.29 (a)	F_J184732.6-011338	31.393	0.299	0.38	6.96	6.6	2460	No
G031.97+00.07 (b)	F_J184922.1-005038	31.943	0.074	0.42	0.88	6.9	420	Yes
G031.97+00.07 (c)	F_J184926.9-005002	31.961	0.061	0.35	0.82	6.9	490	No
G033.69–00.01 (e)	E_J185248.6+003602	33.623	-0.036	0.32	1.76	7.1	690	No
G033.69–00.01 (b)	E_J185252.6+003832	33.663	-0.032	0.38	1.60	7.1	620	No
G033.69–00.01 (c)	E_J185253.8+004120	33.701	-0.012	0.37	1.35	7.1	530	No
G033.69–00.01 (a)	E_J185257.0+004302	33.743	-0.012	0.38	7.05	7.1	2750	Yes
G034.43+00.24 (a)	F_J185318.9+012650	34.431	0.241	0.34	1.20	3.7	100	Yes
G038.95–00.47 (a)	F_J190407.5+050844	38.959	-0.469	0.53	4.58	2.7	290	Yes
G048.52–00.47 (a)	F_J192207.4+133713	48.519	-0.467	0.38	0.76	2.8	50	No
G048.65–00.29 (a)	F_J192144.7+134925	48.658	-0.289	0.34	1.97	2.5	100	Yes

^a Flux integrated over the area of the object as defined by Clumpfind Di Francesco et al. (2008)

SCUBA Legacy Catalogue after applying our noise cut is 50 mJy beam⁻¹. We plot the limiting contrast of the SCUBA Legacy Catalogue as a function of temperature, derived using equation 7, in Fig. 7. We also plot the forecast sensitivity of the SCUBA-2 Legacy Survey SASSy (the SCUBA-2 “All Sky” Survey; Thompson et al. 2007) and JPS (the JCMT Plane Survey; Moore et al. 2005), which will be discussed further in Section 4.6.

Fig. 7 shows that the median sensitivity of the SCUBA Legacy Catalogue would be sufficient to detect the majority if the Simon et al. (2006) IRDC cores if they have temperatures greater than 10 K. At this temperature we would detect IRDC cores with peak contrast greater than 0.15. This corresponds to the approximate completeness limit of the Simon et al. (2006) catalogue, where the turnover in peak contrast occurs. In our sample of 205 IRDCs within the SCUBA Legacy Catalogue 94% have peak contrast values greater than or equal to 0.15.

The IRDC cores that are not detected at 850 μ m are thus consistent with being low temperature, low column den-

sity cores but below the 0.1 Jy pixel⁻¹ noise cut we applied to the SCUBA Legacy Catalogue. Fig. 7 shows that if they are true clouds they are likely to have temperatures less than 10 K. Almost none were identified with 24 μ m MIPS-GAL sources, corroborating our low temperature hypothesis and implying that they are either transient or potentially prestellar cores.

If we consider the cores not detected at 850 μ m, to be low temperature, low column density cores, this requires that they have a temperature lower than \sim 10 K, whereas the lowest contrast objects in the sample could have temperatures less than 14 K. Typical temperatures for IRDCs range from 8–25 K (Carey et al. 1998; Teyssier et al. 2002; Pillai et al. 2006). However as we do not know how IRDC cores are arranged in temperature we cannot know if we ought to have detected the majority of these objects or not. We therefore cannot rule out the presence of a cold faint transient or prestellar population within the SCUBA non-detected sample, particularly at low contrast values where SCUBA is least sensitive. Recent theoretical mod-

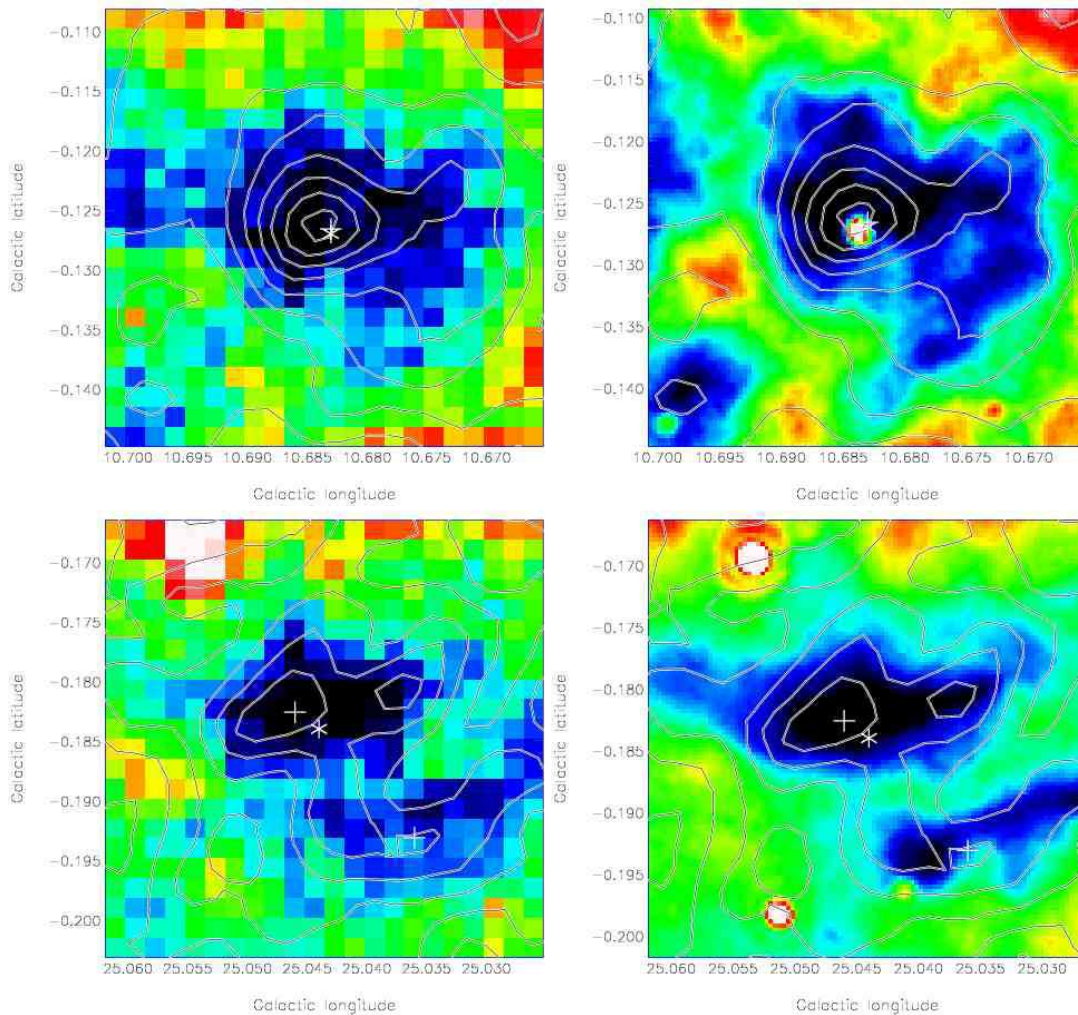


Figure 6. Images of two IRDC cores (top and above) identified in the SCUBA Legacy Catalogue. Images to the left are MSX 8 μm and images to the right are MIPS GAL 24 μm . In each image a star marks the location of the MSX identified candidate IRDC core and the cross marks location of the SCUBA Clumpfind object. Contours in all cases are SCUBA 850 μm . Top: Image of IRDC core: MSXDCG10.71-00.16 (b). Bottom: Image of IRDC core: MSXDCG025.04-00.20 (f).

els (Stamatellos et al. 2007) suggest that the temperature of prestellar cores may be lower than suspected ($\sim 5\text{--}10\text{ K}$), which would place the 850 μm fluxes of the IRDC cores below our detection limit.

An alternative hypothesis is that a number of the cores not detected at 850 μm are a result of the absence of background mid-infrared emission rather than its extinction by intervening cold dust in an IRDC. In this case some of the cores not detected at 850 μm would be localised “holes” or local minima in the mid-infrared background masquerading as IRDCs. This possibility is more likely for the higher contrast cores not detected at 850 μm , as our temperature constraints for these objects mean that they are less likely to be prestellar. Artefacts may also be present as a result of the background subtraction process, which would result in false IRDC detections particularly in regions of complex emission (Simon et al. 2006). Without deeper submillimetre continuum or molecular line data it is difficult to satisfactorily determine whether an IRDC core identified by Simon et al. (2006) and not detected at 850 μm is a true cloud, void or artefact.

4.3 Cores detected at 850 μm

We identified 154 cores detected at 850 μm within the area covered by the SCUBA Legacy Catalogue. These cores have higher peak contrast values (as seen in Fig. 2) and column densities than those cores not detected at 850 μm . Clearly as these objects are seen in submillimetre emission they are not voids or artefacts in the MSX contrast images. We determine estimates of the mass of the 33 cores in our sample with kinematic distances (see Section 2.3). The median mass of cores within the sample is $300 M_{\odot}$, with a minimum mass of $50 M_{\odot}$ and a maximum mass of $4,190 M_{\odot}$ (assuming a dust temperature of 15 K). Our results are consistent with those of Rathborne et al. (2006), who observed the 38 highest contrast clouds from Simon et al. (2006) at 1.2 mm, taking into account differences in sample selection, assumed temperature and in the measurement of integrated fluxes (Rathborne et al. 2006 fit Gaussians to their sample whereas the SCUBA Legacy Catalogue uses Clumpfind).

Are these masses consistent with high mass star formation within the IRDCs? There is considerable uncertainty

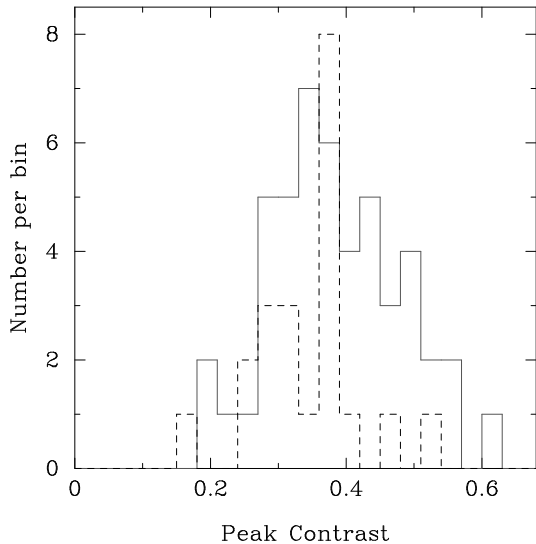


Figure 5. Histogram showing the distribution of the 69 cores detected at 850 μm within the MIPS GAL coverage area with (solid line) and without (dashed line) an embedded 24 μm object at each Peak Contrast value. Bin size used is 0.03.

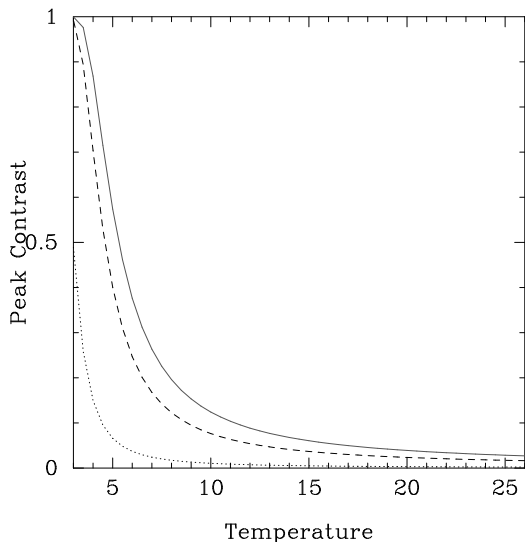


Figure 7. A graph to show the sensitivity of SCUBA at 850 μm (solid line) with respect to the detection of contrast values as a function of core temperature. The dashed line represents the predicted sensitivity of SASSy, which at 3σ will equal 90 mJy. The dotted line represents the predicted sensitivity of JPS, which at 3σ will equal 12 mJy.

regarding the minimum mass core needed to form a high mass star, by considering the observed range in star formation efficiencies Thompson et al. (2006) estimated that a core mass of at least 30–200 M_{\odot} would be required to form a 10 M_{\odot} star. Observed values for high mass star forming cores range from 720 M_{\odot} to $10^4 M_{\odot}$ (Hatchell et al. 2000; Mueller et al. 2002). Our sample of SCUBA detected IRDC cores falls at the lower end of this observed range of masses and is largely consistent with the estimate of the mass required for high mass star formation. We thus conclude that the masses of the IRDC cores in our sample are sufficient to support intermediate to high mass star formation.

4.4 IRDC cores detected at 850 μm without 24 μm sources: could they be “starless” IRDCs?

Approximately two thirds of the IRDC cores detected at 850 μm that are located within the MIPS GAL survey area are associated with embedded 24 μm sources (48 cores or 69% of the sample), as shown in Section 3.3. We carried out KS tests of the peak contrast and column density distributions for SCUBA detected IRDC cores with and without associated 24 μm sources. There is no evidence for the existence of two populations (see Fig. 5), which implies that the IRDC cores detected at 850 μm with and without associated 24 μm sources originate from the same column density population. We searched for any signs of correlation for the limited sample of those cores with known kinematic distances (see Table 3) and did not find any correlation of the presence of an embedded object at 24 μm with the mass of the IRDC core.

Given the similar properties of the cores with and without associated 24 μm sources, the two types of core may be evolutionarily related. The cores that are without associated 24 μm sources could represent an earlier “starless” evolutionary stage to the IRDC cores that have formed intermediate or high mass Young Stellar Objects and are associated with 24 μm sources. A range of evolutionary stages have been observed in a handful of IRDCs (Rathborne et al. 2008), which supports this hypothesis. In this picture the “starless” IRDC cores (i.e. those without associated 24 μm sources) represent the cold quiescent initial conditions for high mass star formation as suggested by Carey et al. (1998) and Simon et al. (2006). The SCUBA detected candidate IRDC cores with associated MIPS GAL 24 μm sources would then represent a star forming population of IRDCs with embedded (proto) stellar objects, and so we refer to these as star forming IRDCs.

Two alternative explanations are that the starless IRDC cores detected at 850 μm are sterile, possibly unbound, condensations that may never go on to form stars, or that they are forming stars, but with luminosities too low to be detected by MIPS GAL. In order to address the likelihood of the former explanation in detail, we would need to determine the virial masses and gravitational stability of a large sample of the starless IRDC cores (via additional spectroscopy). However we note that the Jeans Mass for a core of similar temperature and number density to the starless cores (~ 15 K and 10^4 cm^{-3}) is 20 M_{\odot} . Decreasing the temperature or increasing the number density decrease the Jeans mass. The minimum mass of our sample of cores detected at 850 μm (with or without associated 24 μm sources) is 50 M_{\odot} . Allowing for uncertainties in our derivation of the mass we thus conclude that it is unlikely that many of the IRDC cores fall below this Jeans Mass and so the majority of the IRDC cores detected at 850 μm ought to at least have the potential for star formation.

This approach implicitly assumes that the IRDC cores are single gravitationally bound objects. If instead they are composed of numerous smaller cores fragmented below the scale of the JCMT beam then this conclusion may not apply. Higher resolution interferometry would be needed in this case (e.g. Rathborne et al. 2008).

To assess the likelihood of the latter explanation that the starless IRDC cores are forming stars with luminosities

below the detection limit of MIPS GAL we need to determine the sensitivity of MIPS GAL to YSOs as a function of YSO luminosity. Fortunately a series of studies carried out by the Spitzer c2d⁶ survey team on nearby star forming regions allows us to characterise the 24 μm flux to total internal YSO luminosity fairly well for low mass YSOs. Dunham et al. (2008) find an approximately linear relationship between the MIPS 24 μm flux and total internal luminosity for low mass YSOs detected in the Spitzer c2d survey. This was found to be consistent with the predictions of radiative transfer models of low mass YSOs (Crapsi et al. 2008). Unfortunately no such similar study exists for high mass YSOs and so we use the empirical mid to far-infrared flux relation of Lumsden et al. (2002). We plot these relationships (corrected for an estimate of the average 24 μm extinction of the IRDCs) for a range of YSO luminosities as a function of distance in Fig. 8.

Uncertainties in Fig. 8 result from uncertainties in extinction and in the relationships between flux and luminosity as taken from Lumsden et al. (2002) and Dunham et al. (2008). The main source of error in Dunham et al. (2008) is the uncertainty in the relationship between flux and luminosity which were obtained from observations as well as theoretical models. This uncertainty is depicted in Fig. 8 by the shaded region in the plots on the left. The primary source of error in Lumsden et al. (2002) is due to the large range in observed flux ratio. This uncertainty is depicted in the middle and right plots with the lower estimate in the middle plots and the upper estimates in the plots on the right. From Fig. 8 we see that the relationships taken from Lumsden et al. (2002) and Dunham et al. (2008) are consistent with each other particularly the plots to the right and in the middle of Fig. 8.

The quoted 5σ point source sensitivity of MIPS GAL is 1.7 mJy at 24 μm (Carey et al. 2007). This limit will obviously vary from region to region depending upon the strength of the background emission and complexity of structures in the images. However the IRDCs presented here in general have low 24 μm backgrounds and are relatively free from source crowding, hence we assume the given 5σ limit is valid, which is shown in Fig. 8 by a dashed horizontal line.

The effect of extinction from the environments surrounding the cores found without associated 24 μm emission and from the material contained within the cores themselves lowers any observed radiation emitted from within. With these starless IRDC cores having high column densities ($\sim 2 \times 10^{22} \text{ cm}^{-2}$ from 8 μm and 850 μm data) and hence high opacities there are three possible situations we should consider for the flux that is observed: *i*) there may be no extinction *ii*) there may be a medium amount of extinction (taking this from the lower of the quoted column densities derived from the 8 μm data) *iii*) there may be high extinction (taking this from the higher of the quoted column densities as derived from the 850 μm data). We derive values of visual extinction (A_v) for the two latter cases where extinction has an effect on the observed flux using the method given by Rieke & Lebofsky (1985). The derived A_v range between 11 and 94 which converts to a 24 μm extinction (A_{24})

of 0.6 and 4.6 respectively. The effect of the differing extinction can be seen in Fig. 8 in which the top graphs are for no extinction, the middle graphs take the medium extinction case ($A_{24} = 0.6$), and the bottom graphs assume high extinction ($A_{24} = 4.6$). Errors on these estimates are on the order of $\sim 40\%$, predominantly resulting from the uncertainty in the empirically derived conversion from $N(\text{H}+\text{H}_2)/E(\text{B}-\text{V})$ (Bohlin et al. 1978).

At the typical distance of IRDCs within our Galaxy, which is 3.8 kpc, we look at the sensitivity of MIPS GAL. In Fig. 8, we see that in the ‘worst case scenario’ MIPS GAL should be complete to embedded objects with luminosities above $100 L_\odot$ (when high mid-infrared extinction is considered; $A_{24} = 4.6$, $A_v = 94$). This completeness limit indicates the possibility of ruling out the presence of all but low mass YSOs. From Iben (1965) we find that in the protostellar stages of evolution a star with a final main sequence mass $< 2 M_\odot$ will never reach luminosities greater than $100 L_\odot$. Greater constraints on the column densities of these objects are required to allow us to have a better handle on the potential luminosities of these cores and determine if indeed they are a low mass population of cores.

4.5 The lifetimes of starless and star forming IRDCs

From the previous section we have seen that the starless cores may be evolutionary related to those SCUBA detected cores associated with 24 μm objects but with luminosities below the detection limit of MIPS GAL. Going one step further we may assume that the starless and star forming SCUBA detected IRDCs are at different evolutionary stages in the formation of high mass stars and so we can estimate the statistical lifetime of the starless quiescent phase. If each starless IRDC core evolves into a corresponding star forming IRDC core with one or more embedded 24 μm source then the relative proportions of these objects in the sample should reflect the statistical life time of each type of object. In the sample of SCUBA detected IRDCs lying within the MIPS GAL survey area we find twice as many star forming IRDC cores with 24 μm sources than starless IRDC cores. Thus if these two types of object do form an evolutionary sequence we would expect the starless phase to last half the lifetime of the star forming phase.

Estimates for the absolute lifetime of the embedded high mass star formation range from 10^4 – 10^5 years for UCHII and embedded YSOs (Wood & Churchwell 1989a,b), a few 10^4 years for methanol masers (van der Walt 2005), and 1.2 – 7.9×10^4 years for embedded high mass protostars (Motte et al. 2007; Pestalozzi et al. 2007). Taking the upper and lower bounds of these estimates we conclude that the starless phase of IRDCs, as an upper limit due to our assumption on evolution, last a few 10^3 – 10^4 years. The proportions of starless and star forming IRDCs that we see are consistent with the proportion of massive infrared quiet high mass protostars to the massive protostellar stage as found in Cygnus X by Motte et al. (2007). The lifetime of the starless IRDC phase is comparable to that found for the infrared quiet protostellar phase by Motte et al. (2007) who calculated the statistical lifetimes based on the proportion of massive infrared quiet high mass protostars to the massive protostellar stage as found in Cygnus X. Our sta-

⁶ The Spitzer Space Telescope Legacy program From Molecular Cores to Planet-Forming Disks (Evans et al. 2003)

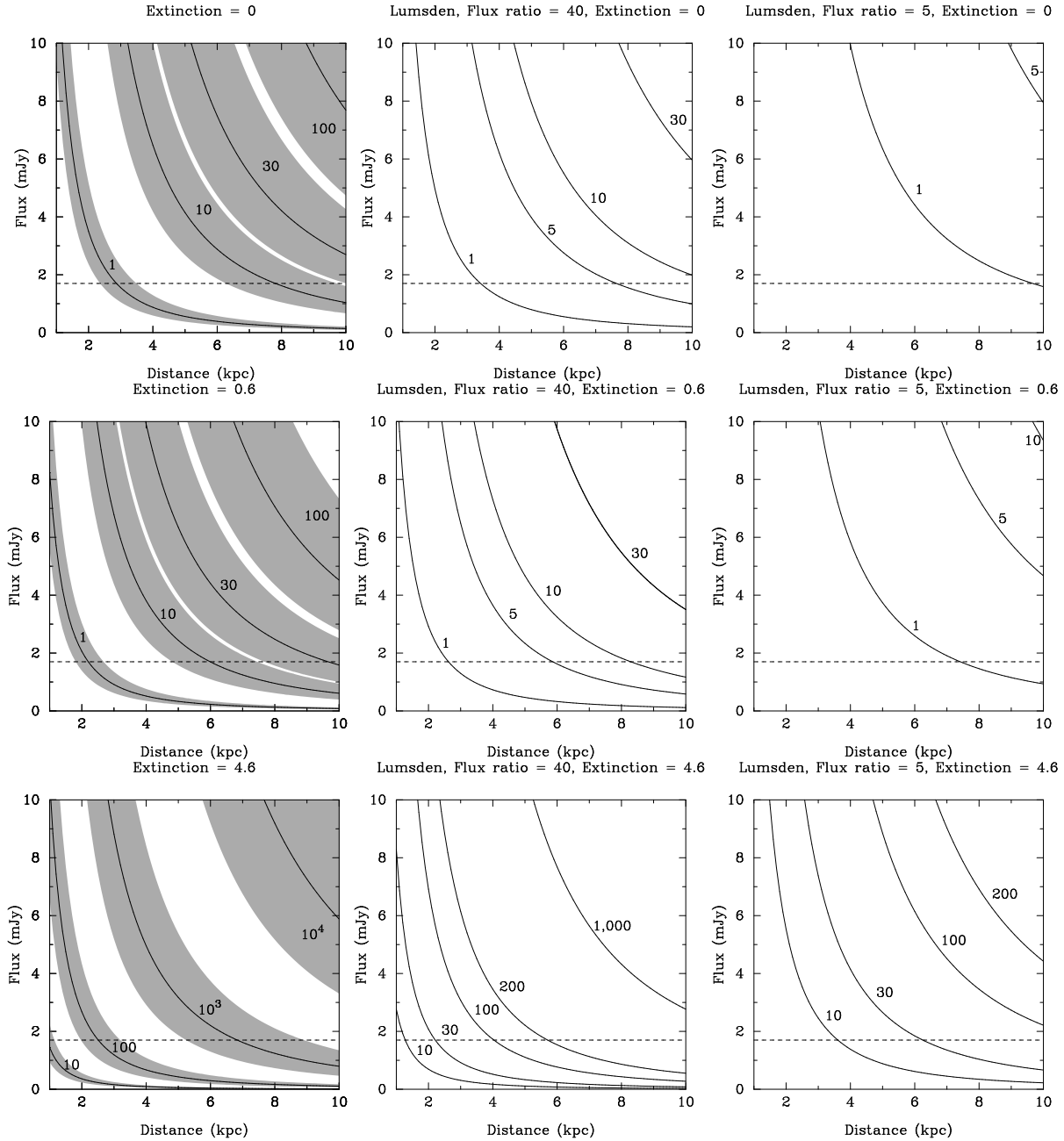


Figure 8. Left Plots: based on relationship between flux and luminosity, from observations and theoretical models as produced in Dunham et al. (2008). The shaded regions depict the uncertainty in this relationship. Middle and Right Plots: based on flux luminosity relationship published by Lumsden et al. (2002). Lower and upper estimates of flux for particular luminosities are plotted in the middle and right plot respectively. This range in flux originates from an observed range in F_{FIR}/F_E ratio which ranges from 5-40. The middle plot takes the value of 40 and the right plot takes the value of 5. Plots from top to bottom vary in A_{24} , from no extinction in the left to high extinction in the right plot. Labels in each plot denote the different luminosities, i.e. $1 L_{\odot}$, $10 L_{\odot}$, $30 L_{\odot}$ and $100 L_{\odot}$. The dashed horizontal line is the 5σ point source sensitivity of MIPS GAL at $24 \mu\text{m}$.

tistical lifetime estimate for the starless IRDC phase is also approximately one to two orders of magnitude less than the extended lifetime of the low mass Class 0 evolutionary phase recently calculated by Evans et al. (2008).

Caution must be applied to comparing the estimated lifetime of starless IRDCs to the estimated lifetime of the high mass pre-stellar phase. As shown by Motte et al. (2007) for Cygnus X there are no high mass starless cores, which implies an age of less than 10^3 years for this phase. The

“starless” IRDCs that we identify from their mid-infrared quietness may yet display other signs of star formation such as molecular outflows or methanol masers which would imply that they have a proto-stellar nature. This may be supported by the fact that their statistical lifetime is similar to the high mass proto-stellar phase identified by Motte et al. (2007). Future investigations of these clouds to search for identifiers of high mass star formation are needed to estimate the lifetimes of the pre-stellar and proto-stellar phases found

within these clouds. A number of forthcoming Galactic Plane surveys have these aims, such as the Methanol Multi Beam Survey (MMB; Green et al. 2008), the CORNISH⁷ 5 GHz survey (Purcell et al. 2008), the Herschel Hi-Gal Survey (Molinari et al. 2005), and the JCMT Legacy Surveys SASSy and JPS (Thompson et al. 2007; Moore et al. 2005), see Section 4.6. However, regardless we have shown that the lifetime of a quiescent (before it shows evidence of activity in the mid-infrared) IRDC is approximately half of that spent in the embedded phase.

4.6 Predictions and implications for Galactic Plane surveys

The astronomical community are planning a number of uniform and sensitive surveys of the Galactic Plane in the far infrared and sub millimetre that will detect a large number of the Simon et al. (2006) IRDC catalogue in emission. We use the results drawn from the SCUBA Legacy Catalogue to make predictions for the number of IRDCs that will be detected by four surveys in particular: SASSy, the SCUBA-2 ‘‘All Sky’’ Survey (Thompson et al. 2007), JPS, the JCMT Galactic Plane Survey (Moore et al. 2005), Hi-GAL, the Herschel Infrared Galactic Plane Survey (Molinari et al. 2005), and ATLASGAL the APEX Telescope Large Area Survey of the Galaxy (Schuller et al. 2009). Each of these surveys will cover much larger regions of the plane than the SCUBA Legacy Catalogue and will be both deeper and more uniform, resulting in a much more unbiased survey of IRDCs that is free from the targeted and non-uniform nature of the SCUBA Legacy Catalogue. Fig 9 shows a region of the Galactic Plane with the coverage area of the SCUBA Legacy Catalogue and the positions of Simon et al. (2006) IRDCs, which clearly indicate the potential of these large area surveys to detect a large number of IRDCs.

As each of these surveys will detect IRDC cores by their emission rather than their extinction against the galactic mid-infrared background this means that they will also be sensitive to IRDCs located on the far side of the Galaxy that were not detected by Simon et al. (2006). The forecast 1σ sensitivities of HiGAL and JPS are 20 mJy beam^{-1} and 4 mJy beam^{-1} at $250 \mu\text{m}$ and $850 \mu\text{m}$ respectively, which are sufficient to detect cores of only a few tens of M_{\odot} at 20 kpc (assuming 20 K dust with $\beta=2$ and a mass coefficient of 50 g cm^{-2}). SASSy and ATLASGAL will have 1σ sensitivities of 30 mJy beam^{-1} and $50\text{--}70 \text{ mJy beam}^{-1}$ at $850 \mu\text{m}$ which could detect cores of a few hundred M_{\odot} out to 20 kpc. Taking the masses of known IRDC cores into consideration each of these surveys has the potential to detect these objects at the far side of the Galaxy. In addition, as we have shown in Section 4.2, the deeper surveys may find the low column density low temperature clouds that were not detected at $850 \mu\text{m}$ in the SCUBA Legacy Catalogue. Thus as well as the increased number of detections resulting from surveying a larger area of the plane, we expect that the surveys will also detect a greater number of ‘IRDC cores’ on the far side of the Galaxy and the colder population that we have not detected with SCUBA.

Estimating an upper limit to the number of IRDC cores that could be detected by the surveys is difficult. For the IRDC cores located on the far side of the Galaxy that have foreground emission preventing them being detected by Simon et al. (2006) we may estimate their number by geometric means and considering the volume of the Galaxy probed by MSX. Following the argument presented by Rathborne et al. (2006) we estimate that the total number of IRDC cores in the Galaxy may be up to a factor of 3 greater than those detected by Simon et al. (2006). To this number must be added an uncertain quantity of low column density cores whose intrinsic contrast falls below the Simon et al. (2006) criteria for detection but whose column density is great enough to be detected by the surveys (particularly Hi-GAL and JPS). We see from Fig. 10 that the steep turnover of IRDC cores at low contrast values may indicate that the catalogue is incomplete at low contrasts. Without further information on the general temperature distribution of IRDCs it is currently not possible to place firm limits on the number of such cores and so whilst we note that the deeper surveys will detect this colder population (and Hi-GAL will determine the temperature distribution of IRDC cores) we do not include them in our estimate.

Currently no information exists on the temperature distribution of IRDCs in general, as by the nature of their detection the estimated temperature for each cloud is an upper limit. This means that we cannot take the column densities estimated from the MSX $8 \mu\text{m}$ data (as contained in Table 1) and convert these into flux estimates, as the lack of temperature information renders these into rather loosely determined upper flux limits. In addition the large uncertainties in mass coefficients, the $8 \mu\text{m}$ extinction law and contamination from foreground emission introduce a considerable scatter between column densities derived from $8 \mu\text{m}$ and $850 \mu\text{m}$ (see Section 2.3). We thus estimate lower limits for the detection rate of IRDC cores within the surveys by using the SCUBA detection fraction shown in Section 4.1. SASSy, JPS and Hi-GAL are deeper than the SCUBA Legacy Catalogue and so we expect these surveys to detect a greater fraction of IRDC cores, particularly at low contrast values where the surveys are more sensitive to low temperature low column density cores (see Fig. 7). Without knowing the temperature distribution of IRDC cores it is impossible to determine exactly what this fraction is, but given the greater sensitivities of these surveys they ought to detect at least the fraction of IRDC cores that SCUBA did. The depth of ATLASGAL is similar to the $0.1 \text{ Jy pixel}^{-1}$ noise cut that we applied to the SCUBA Legacy Catalogue and thus ATLASGAL should detect a similar fraction of IRDC cores from Simon et al. (2006).

ATLASGAL will survey the inner third of the Galactic Plane ($|l| < 60^{\circ}$ and $|b| < 1.5^{\circ}$), within which there are 11,529 IRDC cores from the Simon et al. (2006) catalogue. Taking the SCUBA detection fraction of 75% we predict that ATLASGAL will detect at least 8,600 IRDC cores. We scale this number by the geometric argument of Rathborne et al. (2006) to estimate the number of cores that ATLASGAL will detect on the far side of the Galaxy and hence estimate that ATLASGAL may detect up to 26,000 IRDC cores. This is consistent with the preliminary results of the first 95 deg² of ATLASGAL which detects $\sim 6,000$ sources, many of them infrared dark (Schuller et al. 2009).

⁷ The Co-Ordinated Radio ‘N’ Infrared Survey for High-mass star formation, Purcell et al. (2008)

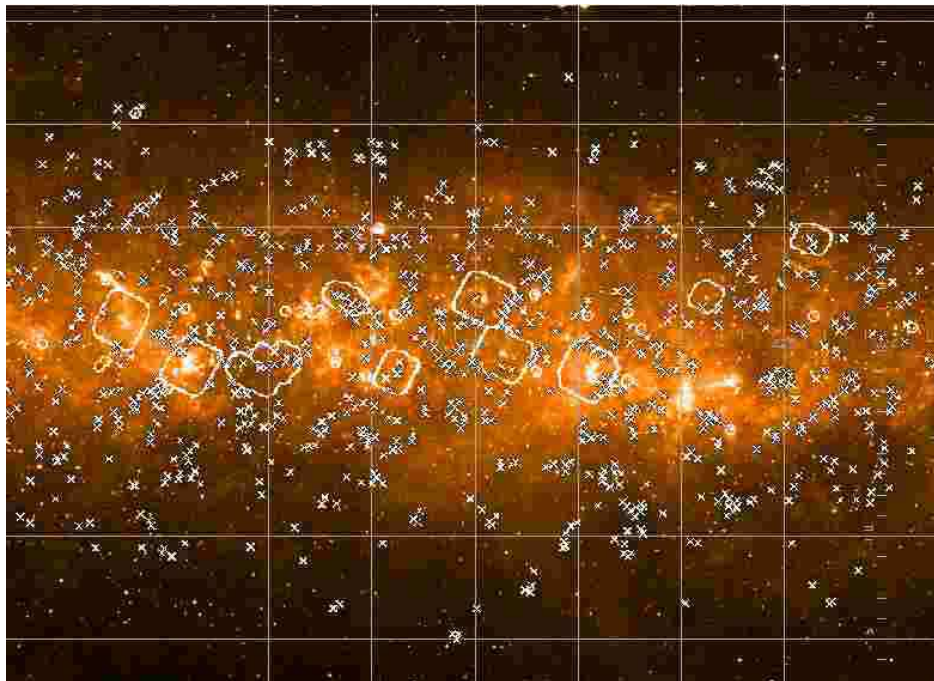


Figure 9. Image of a region of the Galactic plane. MSX $8\ \mu\text{m}$ image with SCUBA coverage area contours overlaid. The crosses mark the locations of potential IRDC cores as catalogued by Simon et al. (2006).

The survey area of Hi-GAL again covers the inner third of the Galactic Plane but with a latitude range $|b| < 1^\circ$. Of the 12,774 cores within the IRDC core catalogue by Simon et al. (2006) 10,644 IRDC cores are located within the Hi-GAL survey area. Scaling this to the detection fraction of SCUBA Hi-GAL will detect at least 8,000 IRDC cores. Again we use the geometric argument to estimate that within the entire Galaxy this number may increase to 24,000 cores. SASSy, covering $0^\circ \leq l \leq 245^\circ$ and $|b| \leq 5^\circ$ of the Galactic plane has 6,160 IRDC cores from the Simon et al. (2006) within the coverage area. Taking the 75% detection fraction results in a lower estimate of 4,600 cores being observed. Again the number detected increases, when we consider geometric arguments, to 14,000. Finally JPS will survey two regions of the Galactic Plane, the GLIMPSE-N region ($10^\circ < l < 65^\circ$ and $|b| \leq 1^\circ$) and the FCRAO Outer Galaxy Survey region ($102.5^\circ < l < 141.5^\circ$ and $|b| \leq 1^\circ$). We see that 4,095 IRDC cores from Simon et al. (2006) are located within the coverage area. With a detection fraction of 75% we expect a lower limit of 3,000 IRDC cores to be detected. With geometric arguments this number may increase to 9,000 IRDC cores. Although by number we see that the predicted numbers of IRDC cores that ATLASGAL and Hi-GAL are expected to return higher source counts than SASSy and JPS, this is due to the larger area covered by these surveys. JPS and SASSy will however explore relatively unique parameter spaces. The high sensitivity JPS ($1\sigma \sim 4\ \text{mJy beam}^{-1}$ at $850\ \mu\text{m}$) will be ideal for identifying the most low temperature low column density IRDC cores. SASSy in contrast to the other surveys will have the benefit of observing greater latitudes of the Galactic Plane than any other survey and (as with JPS) will observe the outer Galaxy where low mid infrared backgrounds has restricted previous identifications of ‘IRDCs’ due to their very nature.

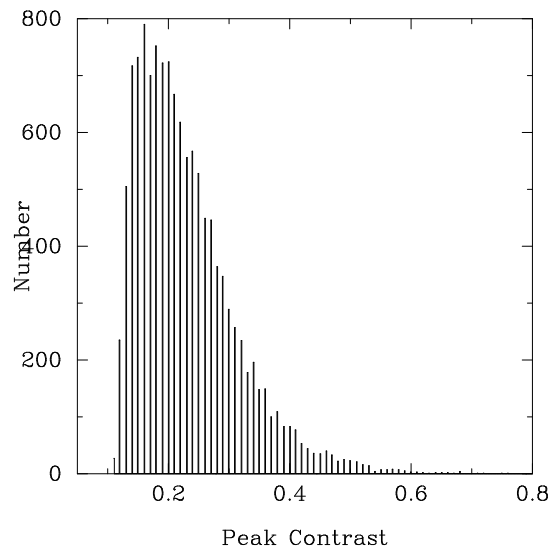


Figure 10. Number distribution of IRDC cores with peak contrasts, values taken from Simon et al. (2006).

5 SUMMARY AND CONCLUSIONS

From positional cross matching of the IRDC catalogue produced by Simon et al. (2006) with the coverage area of the SCUBA Legacy Catalogue (as published by Di Francesco et al. 2008) we have identified two populations of objects: candidate IRDC cores with and without associated $850\ \mu\text{m}$ emission. Column densities of these two populations were derived from the $8\ \mu\text{m}$ data by applying an extinction law to the peak contrast values (as defined by Simon et al. 2006 based upon observations at $8\ \mu\text{m}$). For those cores that were associated with $850\ \mu\text{m}$ emission col-

umn densities were also derived assuming a spherical geometry and the assumption of Hildebrand (1983). From our findings outlined within this paper we make the following conclusions:

(i) We find 154 cores with 850 μm detected emission and 51 cores without 850 μm emission. Those cores associated with detectable 850 μm emission had a median peak contrast value of 0.32, a median column density of $1.7 \times 10^{22} \text{ cm}^{-2}$ and a median mass of $300 M_{\odot}$. We found that the overall detection fraction of IRDC cores with 850 μm emission is 75%, as a lower limit which is in good agreement with the CS detection of Jackson et al. (2008).

(ii) Those cores without 850 μm emission are found to have no significant difference in peak contrast distribution than those cores detected at 850 μm . These cores are likely to be population of low temperature low column density transient or prestellar cores. However, a small number of these cores could also be “holes” in the background mid-infrared continuum emission or artefacts as a result of the identification procedure. Further observations of the cores not detected at 850 μm , either deeper sub millimetre continuum data or molecular line data, are required to yield insight into the true nature of these objects.

(iii) On the nature of those cores detected at 850 μm , we find that their range in masses ($50 - 4,190 M_{\odot}$) are consistent with the lower mass end range observed in high mass star forming regions. 69% of those cores detected at 850 μm lying within the MIPS GAL survey area are associated with an embedded object at 24 μm . A KS test gave no indication for the existence of two populations. This could suggest these cores are related evolutionarily. Those cores detected at 850 μm without 24 μm sources could be “starless” IRDCs or they may be forming stars but with luminosities too low to be detected. An alternative explanation for their origins are that they are unbound condensations that may never go on to form stars. To make more detailed conclusions about the nature of the SCUBA detected cores and their embedded mid-IR sources requires a deeper understanding of their physical properties from follow up molecular line mapping.

(iv) Based on the assumption that the “starless” and star forming cores are related evolutionarily we derive an upper limit of $10^3 - 10^4$ years for the lifetimes of starless IRDC cores. This lifetime is found to be comparable to the infrared quiet protostellar phase by Motte et al. (2007) and is approximately one to two orders of magnitude less than the extended lifetime of the low mass Class 0 evolutionary phase recently calculated by Evans et al. (2008).

(v) Based on SCUBA detection rates found, we make a conservative prediction to a lower limit of the number of IRDC cores that the Galactic Plane surveys ATLASGAL, Hi-GAL, SASSy and JPS will potentially detect : 8,600, 8,000, 4,600 and 3,000 cores respectively. If we apply geometric arguments to these values to scale to the number of such cores in the far Galaxy (Rathborne et al. 2006) we see that ATLASGAL, Hi-GAL, SASSy and JPS have the potential to observe up to 26,000, 24,000, 14,000 and 9,000 infrared dark cores respectively throughout the Galaxy.

We are now entering into an exciting time for sub millimetre and far infrared astronomy with the advent of Herschel and SCUBA-2. These two instruments will push the observational investigations of IRDCs, and in turn they will

yield fresh insight into the role they may play in massive star formation

ACKNOWLEDGMENTS

We thank the STFC and the University of Hertfordshire for support and an anonymous referee for a number of useful comments that substantially improved this work. We also thank James Fi Francesco for providing a file of all SCUBA Legacy Catalogue noise values. This research has made use of NASA’s Astrophysics Data System. We would also like to acknowledge the JCMT (The James Clerk Maxwell Telescope is operated by The Joint Astronomy Centre on behalf of the Science and Technology Facilities Council of the United Kingdom, the Netherlands Organisation for Scientific Research, and the National Research Council of Canada), MIPS GAL and Midcourse Space Experiment. This research used the facilities of the Canadian Astronomy Data Centre operated by the National Research Council of Canada with the support of the Canadian Space Agency.

REFERENCES

- Bohlin R. C., Savage B. D., Drake J. F., 1978, *ApJ*, 224, 132
- Carey S. J., Clark F. O., Egan M. P., Price S. D., Shipman R. F., Kuchar T. A., 1998, *ApJ*, 508, 721
- Carey S. J., Mizuno D. R., Kraemer K., Shenoy S., Noriega-Crespo A., Price S. D., Paladini R., Kuchar T., 2007, MIPS GAL documentation
- Chambers E. T., Jackson J. M., Rathborne J. M., Simon R., 2009, *ApJS*, 181, 360
- Crapsi A., van Dishoeck E. F., Hogerheijde M. R., Pontopidan K. M., Dullemond C. P., 2008, *A&A*, 486, 245
- Di Francesco J., Johnstone D., Kirk H., MacKenzie T., Ledwosinska E., 2008, *ApJS*, 175, 277
- Du F., Yang J., 2008, *ApJ*, 686, 384
- Dunham M. M., Crapsi A., Evans II N. J., Bourke T. L., Huard T. L., Myers P. C., Kauffmann J., 2008, *ApJS*, 179, 249
- Egan M. P., Shipman R. F., Price S. D., Carey S. J., Clark F. O., Cohen M., 1998, *ApJL*, 494, L199+
- Evans II N. J., Allen L. E., Blake G. A., et al. 2003, *PASP*, 115, 965
- Evans II N. J., Dunham M. M., Jørgensen J. K., et al. 2008, *ArXiv e-prints*
- Frieswijk W. F., Spaans M., Shipman R. F., Teyssier D., Carey S. J., Tielens A. G. G. M., 2008, *ArXiv e-prints*, 808
- Green J. A., Caswell J. L., Fuller G. A., et al. 2008, *ArXiv e-prints*
- Hatchell J., Fuller G. A., Millar T. J., Thompson M. A., Macdonald G. H., 2000, *A&A*, 357, 637
- Hildebrand R. H., 1983, *QJRAS*, 24, 267
- Iben I. J., 1965, *ApJ*, 141, 993
- Jackson J. M., Chambers E. T., Rathborne J. M., Simon R., Zhang Q., 2008, in Beuther H., Linz H., Henning T., eds, *Massive Star Formation: Observations Confront Theory Vol. 387 of Astronomical Society of the Pacific Conference Series, Infrared Dark Clouds*. pp 44+

- Jackson J. M., Finn S. C., Rathborne J. M., Chambers E. T., Simon R., 2008, *ApJ*, 680, 349
- Kerton C. R., Martin P. G., Johnstone D., Ballantyne D. R., 2001, *ApJ*, 552, 601
- Lumsden S. L., Hoare M. G., Oudmaijer R. D., Richards D., 2002, *MNRAS*, 336, 621
- Molinari S., Swinyard B., Barlow M., Bernard J. P., Boulanger F., Testi L., White G., Hi-Gal Team 2005, in *Protostars and Planets V A Herschel Far Infrared Survey of the Galactic Plane*. pp 8163–+
- Moore T. J. T., Shipman R. F., Plume R., Hoare M. G., Jps International Collaboration 2005, in *Protostars and Planets V Legacy Surveys with the JCMT: The JCMT Plane Survey*. pp 8370–+
- Motte F., Bontemps S., Schilke P., Schneider N., Menten K. M., Broguière D., 2007, *A&A*, 476, 1243
- Mueller K. E., Shirley Y. L., Evans II N. J., Jacobson H. R., 2002, *ApJS*, 143, 469
- Perault M., Omont A., Simon G., et al. 1996, *A&A*, 315, L165
- Pestalozzi M. R., Chrysostomou A., Collett J. L., Minier V., Conway J., Booth R. S., 2007, *A&A*, 463, 1009
- Pillai T., Wyrowski F., Carey S. J., Menten K. M., 2006, *A&A*, 450, 569
- Pillai T., Wyrowski F., Menten K. M., Krügel E., 2006, *A&A*, 447, 929
- Purcell C. R., Hoare M. G., Diamond P., 2008, in Beuther H., Linz H., Henning T., eds, *Massive Star Formation: Observations Confront Theory Vol. 387 of Astronomical Society of the Pacific Conference Series, The CORNISH Survey of the Galactic Plane*. pp 389–+
- Ragan S. E., Bergin E. A., Plume R., Gibson D. L., Wilner D. J., O’Brien S., Hails E., 2006, *ApJS*, 166, 567
- Rathborne J. M., Jackson J. M., Simon R., 2006, *ApJ*, 641, 389
- Rathborne J. M., Jackson J. M., Zhang Q., Simon R., 2008, *ArXiv e-prints*, 808
- Rathborne J. M., Simon R., Jackson J. M., 2007, *ApJ*, 662, 1082
- Rieke G. H., Lebofsky M. J., 1985, *ApJ*, 288, 618
- Schuller F., Menten K. M., Contreras Y., et al. 2009, *ArXiv e-prints*
- Simon R., Jackson J. M., Rathborne J. M., Chambers E. T., 2006, *ApJ*, 639, 227
- Simon R., Rathborne J. M., Shah R. Y., Jackson J. M., Chambers E. T., 2006, *ApJ*, 653, 1325
- Stamatellos D., Whitworth A. P., Ward-Thompson D., 2007, *MNRAS*, 379, 1390
- Teyssier D., Hennebelle P., Pérault M., 2002, *A&A*, 382, 624
- Thompson M. A., Hatchell J., Walsh A. J., MacDonald G. H., Millar T. J., 2006, *A&A*, 453, 1003
- Thompson M. A., Serjeant S., Jenness T., et al. 2007, *ArXiv e-prints*, 704
- van der Walt J., 2005, *MNRAS*, 360, 153
- van der Wiel M. H. D., Shipman R. F., 2008, *ArXiv e-prints*, 807
- Williams J. P., de Geus E. J., Blitz L., 1994, *ApJ*, 428, 693
- Wood D. O. S., Churchwell E., 1989a, *ApJ*, 340, 265
- Wood D. O. S., Churchwell E., 1989b, *ApJS*, 69, 831

This paper has been typeset from a $\text{\TeX}/\text{\LaTeX}$ file prepared by the author.